Order and Disorder in Symmetric Diblock Copolymer Melts

Jeffrey H. Rosedale[†] and Frank S. Bates*

Department of Chemical Engineering and Materials Science, University of Minnesota, Minneapolis, Minnesota 55455

Kristoffer Almdal and Kell Mortensen

Risø National Laboratory, Roskilde, Denmark DK-4000

George D. Wignall

Oak Ridge National Laboratory, Oak Ridge, Tennessee 37831

Received April 13, 1994; Revised Manuscript Received November 8, 1994[⊗]

ABSTRACT: The thermodynamic and dynamic properties of several partially deuterated symmetric (equal block volume fraction) polyethylene–poly(ethylethylene) (PE–PEE), poly(ethylene–propylene)–poly(ethylethylene) (PEP–PEE), and polyethylene–poly(ethylene–propylene) (PE–PEP) diblock copolymers were characterized above and below the order–disorder transition (ODT). A lamellar morphology was established for all temperatures below the ODT using small-angle neutron scattering (SANS) measurements with shear-aligned specimens. As T_{ODT} is approached, the lamellar order weakens as evidenced by the loss of higher order SANS reflections and azimuthal smearing of the principal equitorial scattering peaks. SANS and rheology experiments also provided unambiguous evidence of composition fluctuations above the order–disorder transition temperature in each system. However, the temperature range of the fluctuations in the disordered state depends on the degree of polymerization, in accordance with fluctuation theory. A crossover in the disordered state between slightly and moderately stretched coils was also documented by SANS, coincident with the temperature where fluctuations become apparent rheologically.

I. Introduction

In this paper we report on the structure and rheological properties of symmetric A–B diblock copolymer melts in the vicinity of the order–disorder transition (ODT). At high temperatures, in the homogeneous disordered state, such melts are uniform in composition and the diblock chains obey Gaussian or "random walk" statistics such that $R_g = aN^{1/2}/6$, where R_g is the radius of gyration, N is the number of chain segments, and a is the statistical segment length.[1] As the temperature is lowered, increasing incompatibility between the A and B blocks causes a "microphase separation" or self-assembly of the macromolecules in order to minimize unfavorable contacts between the opposing segments. In this paper the diblocks are compositionally symmetric ($f = 1/2$) and self-assemble, or order, into alternating layers of A-rich and B-rich lamellae. Early theoretical descriptions of the order (lamellar)–disorder transition assumed that the chain statistics remained essentially Gaussian and that the composition profile varied sinusoidally from layer to layer.[2,3] This regime is referred to as "the weak segregation limit" (WSL), and the lamellar domain spacing, d, is predicted to scale as $d \sim R_g \sim N^{1/2}$. However, recent experiments,[4–9] simulations,[10–12] and theories[13–15] indicate that significant deviations from Gaussian conformational behavior ensue far above the ODT in the disordered state. Theories and simulations anticipate a gradual stretching of the diblock coils ($d \sim N^{\delta}$, with $0.7 < \delta < 0.8$) accompanied by an increase in composition fluctuations as the ODT is approached. The magnitude and range of these fluctuation effects are expected to diminish with increasing N.[3,12–15] An objective of the work reported here was to correlate the degree of chain stretching and composition fluctuations with N in various polyolefin diblock copolymers near the order–disorder transition.

Evidence for composition fluctuation effects and non-Gaussian chain conformations in the disordered state was obtained from small-angle neutron scattering (SANS) and low-frequency dynamic mechanical spectroscopy experiments on poly(ethylene–propylene)–poly(ethylethylene) (PEP–PEE) diblock copolymers.[4–8] These results identified the ODT as a fluctuation-induced weakly first-order phase transition and supported the fluctuation theory of Fredrickson and Helfand.[3] This theory was developed by applying a concept originally introduced by Brazovskii[16] to the mean-field treatment of Leibler[2] and is denoted the BLFH theory. For compositionally symmetric ($f = 0.5$) diblocks, BLFH theory predicts

$$(\chi N)_{ODT} = 10.495 + 41.0\bar{N}^{-1/3} \tag{1}$$

where χ is the Flory–Huggins interaction parameter and

$$\bar{N} = Na^6v^{-2} \tag{2}$$

is the finite molecular weight (fluctuation) correction to the mean-field theory, where a and v are the statistical segment length and volume, respectively. In the limit of infinite molecular weight, $\bar{N} \to \infty$, the mean-field result, $(\chi N)_{ODT} = 10.495$, is recovered. The molecular weights of the PEP–PEE diblocks studied earlier[4–8] were approximately 50 000 with $\bar{N} \approx 10^4$ and $(\chi N)_{ODT} \approx 12$. Based on the estimated value of $\chi(T)$ (see text below) the fluctuation regime $\Delta(\chi N) = 41.0\bar{N}^{-1/3}$ for the PEP–PEE system is predicted to extend roughly 70–90 °C above the order–disorder transition temperature, T_{ODT}. According to the BLFH theory, this

* To whom correspondence should be addressed.
[†] Current address: Research Laboratories, Rohm & Haas Company, Bristol, PA 19007.
[⊗] Abstract published in *Advance ACS Abstracts,* February 15, 1995.

0024-9297/95/2228-1429$09.00/0

fluctuation range should be wider in lower molecular weight diblocks and narrower in higher molecular diblocks. Compared to comparable molecular weight binary homopolymer mixtures, this represents an enormous range of non-mean-field behavior.[17] The molecular weight (i.e., $\bar{N}$) dependence of this fluctuations behavior was explored using 10 model symmetric saturated hydrocarbon diblock copolymers: polyethylene–poly(ethylethylene) (PE–PEE) polyethylene–poly(ethylene–propylene) (PE–PEP), and PEP–PEE. The range of molecular weights was 2.8×10^3–1.36×10^4. At 130 °C this translates into a 10-fold variation in $\bar{N}$, $0.3 \times 10^4 \lesssim \bar{N} \lesssim 3 \times 10^4$.

In addition to large differences in $\bar{N}$, these polyolefin diblock copolymers also exhibit differences in conformational asymmetry. Recent reports describe the effects of conformational asymmetry on the thermodynamics of blends of saturated hydrocarbon isomers, such as PE, PEP, and PEE. A chain conformation parameter, β, is defined in terms of the molecular weight independent combination

$$\beta^2 = R_g^2/V = a^2/6v \tag{3}$$

where V refers to the chain volume and R_g is the Gaussian coil dimension. For the polymer blocks used in this study, $\beta_{PE}^2 = 0.13$ Å^{-1}, $\beta_{PEP}^2 = 0.086$ Å^{-1}, and $\beta_{PEE}^2 = 0.050$ Å^{-1}, at 150 °C. In general, β decreases as the degree of chain branching increases because the chain contour length decreases as more and more molecular volume is consumed as pendant groups. We have adopted the notation introduced by Vavasour and Whitmore[20] in characterizing conformational asymmetry in a diblock copolymer,

$$\epsilon = \beta_A^2/\beta_B^2 \tag{4}$$

so that at 150 °C $\epsilon_{PE-PEP} = 1.5$, $\epsilon_{PEP-PEE} = 1.7$, and $\epsilon_{PE-PEE} = 2.6$. An important effect of increasing ϵ in saturated hydrocarbon mixtures and block copolymers is to increase the interaction parameter χ.[18,19] Since this has been linked to conformational effects at length scales between a and R_g in homopolymers,[19] we expect a strong influence in block copolymers that segregate at similar, nonlocal, length scales.

Our experimental approach in investigating the role of $\bar{N}$ on undiluted (bulk) diblock copolymer phase behavior and conformation followed two protocols. Isotropic samples were first studied with dynamic mechanical spectroscopy and small-angle neutron scattering (SANS) techniques to identify the ODT and to study fluctuation and conformational asymmetry (chain stretching) effects in the disordered state. These experiments lead us to conclude that fluctuation effects diminish with increasing $\bar{N}$, in accordance with theory, and that the onset of finite amplitude composition fluctuations is preceded by a departure from the WSL scaling of d. A second class of experiments was conducted with macroscopically oriented (anisotropic) specimens, obtained through the application of large strain amplitude oscillatory shear deformation. These measurements indicate that the lamellar order weakens near T_{ODT}, leading to considerable distortion (e.g., rippling) prior to disordering.

II. Experimental Section

II-A. Synthesis. Butadiene (Aldrich, 99+%) and isoprene (Aldrich, gold label) monomers were purified by successive vacuum distillations from dibutylmagnesium (Johnson-Mattthey) and *n*-butyllithium (Aldrich). Perdeuterated butadiene(-d_6) (MSD Isotopes) was also purified by successive vacuum distillations from sodium metal and *tert*-butyllithium. Cyclohexane (Aldrich, 99%) was stirred over sulfuric acid (Baker, reagent grade) for at least a week to remove any residual alkenes and further purified by distillation from excess poly(styryllithium) for the anionic polymerizations. Cyclohexane (Aldrich, anhydrous, 99+%) was used as received for the hydrogenation (or deuteration) reactions. *sec*-Butyllithium in cyclohexane (Aldrich) was used as received; the active initiator concentration (ca. 1.3 M) was determined by the Gilman double-titration method. Dipiperidinoethane (DiPiP; Aldrich) was purified by successive vacuum distillations from calcium hydride and dibutylmagnesium. Methanol (E M Science) was used as received for polymer precipitations or deoxygenated by successive freeze–pumping for use in polymerization termination. Isopropyl alcohol (E M Science) was also used as received for precipitations.

Anionic polymerization of poly(1,4-butadiene)–poly(1,4-isoprene) diblock copolymers (1,4PB–1,4PI) was conducted under purified argon in a Pyrex reactor fitted with Viton O-ring-sealed joints and Teflon or Viton O-ring-sealed valves. Cyclohexane was distilled directly into the reactor and brought to 40 °C. An aliquot of *sec*-butyllithium was added to the well-stirred solvent with a gas-tight syringe (Hamilton), followed by the immediate addition of isoprene. The total anion concentration ranged from 2.6×10^{-3} to 5.2×10^{-3} mol/L. Polymerization of the isoprene was evidenced by a rise in temperature (ca. 4 °C), which peaked after approximately 25 min, and a drop in the reactor pressure. After 3–4 h (considerably longer than either the anticipated time for >99% conversion or the time at which the reactor pressure ceased dropping) the butadiene was added (the reactor was momentarily cooled to 20 °C for 15 min to prevent reactor overpressure during butadiene addition). Polymerization of butadiene was indicated by a drop in the reactor pressure. Reactions were terminated after 12 h by addition of 2–3 mL of degassed methanol. This procedure gives mostly poly(1,4-isoprene) and poly(1,4-butadiene) (mixture of cis and trans and 1,2 units; see below). The resulting diblock copolymers were recovered by precipitation in a 3:1 (v/v) mixture of methanol and isopropyl alcohol, vacuum dried, and stored in the absence of light under purified argon at −30 °C.

Poly(1,4-butadiene)–poly(1,2-butadiene) diblock copolymers (1,4PB–1,2PB) were similarly prepared with the exception that the 1,2-butadiene block was polymerized for 24 h in the presence of a 5:1 molar ratio of DiPiP to anion at 20 °C. Poly(1,4-isoprene)–poly(1,2-butadiene) (1,4PI–1,2PB) diblock copolymers were prepared using procedures similar to those reported elsewhere.[4]

Each of the diblock copolymers was saturated in separate reactions with either hydrogen or deuterium gas (500 psi) over a palladium catalyst supported on calcium carbonate (Strem Chemical Co.) in a dilute cyclohexane solution (2% w/v) maintained at 70–80 °C. Saturation of 1,4PB–1,4PI, 1,4PI–1,2PB, and 1,4PB–1,2PB yields polyethylene–poly(ethylene–propylene) (PE–PEP), poly(ethylene–propylene)–poly(ethylethylene) (PEP–PEE), and polyethylene–poly(ethylethylene) (PE–PEE) diblock copolymers, respectively. Discussions of this reaction are presented elsewhere.[21] Deuteration of poly(1,4-isoprene) and poly(1,4-butadiene) blocks under these conditions does not lead to the stoichiometric addition of two deuterons to each double bond. In separate reactions with comparable molecular weight poly(1,4-isoprene) homopolymer we found that on average four to five deuterons are associated with each isoprene repeat unit. Deuterium content was determined using density gradient column measurements. Approximately three deuterons add to a 1,2-butadiene repeat unit, and between three and four, to a 1,4-butadiene unit.[22] As a result of the asymmetric addition of deuterium to the individual blocks of the 1,4PB–1,4PI diene precursors, the deuterated PE–PEP products contain an excess of deuterium on the PEP block that provides a sufficient level of neutron contrast to allow for SANS measurements (see below). Higher contrast samples were obtained by hydrogen-saturation of 1,-

Table 1. Diblock Copolymer Characterization

diblock (A−B)	isotope[a]	f_A	10^3M_w	M_w/M_n	N_n[b]	T_{ODT},[c] °C
PE−PEP−1D	(H)D−(H)D	0.50	93.4	1.06	1573	119 ± 1
PE−PEP−2H	(H)H−(H)H	0.49	115	1.07	1919	139 ± 1
PE−PEP−6H	(D)H−(H)H	0.50	128	1.09	1925	139 ± 1
PE−PEP−3D	(H)D−(H)D	0.49	136	1.06	2291	159 ± 1
PEP−PEE−14H	(H)H−(D)H	0.54	47.8	1.08	791	16 ± 2[d]
PEP−PEE−2H	(H)H−(H)H	0.56	53.6	1.07	895	96 ± 1[e]
PEP−PEE−5H	(H)H−(D)H	0.55	57.5	1.05	978	125 ± 1[f]
PEP−PEE−3H	(H)H−(H)H	0.53	85.3	1.05	1451	291 ± 1[e]
PE−PEE−8H	(H)H−(D)H	0.50	27.5	1.15	427	136 ± 2
PE−PEE−1H	(H)H−(D)H	0.48	28.6	1.05	486	182 ± 2

[a] (H)D refers to a hydrogenous diene that was deuterated. [b] $N_n = [M_w \div (M_w/M_n) \div 56]$ (±5%). [c] Based on discontinuity in G' while heating. [d] From anisotropic to isotropic transition in SANS pattern while heating. [e] Reference 8. [f] Reference 6.

4PI−1,4PB-d_6, 1,4PI−1,2PB-d_6, and 1,4PB−1,2PB-d_6 diene precursors.

II-B. Molecular Characterization. Room-temperature ^{1}H NMR spectra were obtained from 5% (w/v) $CDCl_3$ solutions of the PEP−PEE diblock copolymers with an IBM AC-200 spectrometer. High-temperature (90 °C) ^{1}H NMR spectra were also obtained from 5% (w/v) toluene-d_8 solutions of the PE−PEP and PE−PEE diblock copolymers with a Varian VXR-300 spectrometer. The weight-average molecular weights of the PEP−PEE diblocks were determined from light scattering measurements conducted on polymer solutions prepared in THF; a constant flow apparatus operating with a room-temperature THF mobile phase at 1.0 mL/min (Knauer HPLC pump) was used in which the polymer solutions (3.0 mL) pass through Toyo Soda TSK-Gel "Styragel" columns, an Optilab Interference diffractometer fitted with a 0.2 mm flow cell, and a Chromatix KMX-6 low-angle laser light scattering instrument fitted with a 1 cm flow cell. At least three runs of four concentrations of each polymer solution were performed. Weight-average molecular weight determinations were not performed on the PE−PEP and PE−PEE diblocks as a result of the insolubility of the PE blocks in room-temperature THF. Instead, light scattering measurements were performed on the diene precursors dissolved in toluene and injected into the THF mobile phase described above; this procedure minimizes oxidative degradation. Size-exclusion chromatography (SEC) measurements were also performed on the PEP−PEE diblock copolymers (reported elsewhere[4]) and the diene diblock precursors with an instrument fitted with dual Zorbax (Du Pont) size-exclusion columns and operated at room temperature with THF as the mobile phase at a flow rate of 0.5 mL/min. Elution times were monitored with a differential refractometer (Waters) following injection of 100 μL of 0.05% (w/v) polymer solutions prepared in benzene; this prevents degradation, and the benzene acts as an internal elution volume standard. The instrument was calibrated with a series of monodisperse poly(1,4-isoprene) standards (Goodyear) to determine the molecular weight polydispersity, M_w/M_n, of each specimen.

The characteristics of the diblock copolymers used in this study are summarized in Table 1, grouped according to type (PE−PEP, PEP−PEE, and PE−PEE) and in order of increasing molecular weight. All the compositions (volume fraction f_A) are close to being symmetric ($f_A = 1/2$). The overall number-average degree of polymerization, N_n, was calculated using a repeat unit (mer) molecular weight of 56 and corrected for polydispersity and isotopic content. N_n values range from approximately 2000 for PE−PEP to 1000 for PEP−PEE and to 450 for PE−PEE. These were selected to give measurable order−disorder transition temperatures (see rheology results, below). Neutron contrast was obtained using the two synthetic routes indicated above: (i) utilizing the H−D isotope exchange effect that occurs during deuteration of the perhydrogenous diene precursor or (ii) hydrogenating a diene diblock containing a perdeuterous block. The method used for each sample listed in Table 1 is identified in the column labeled "isotope". The letters in parentheses refer to the diene precursor blocks, and the adjacent letter indicates the isotope used in the saturation reaction. For example, PE−PEP-6H is denoted (D)H−(H)H, indicating that the polydiene precursor was prepared with perdeuterous butadiene and hydrogenous isoprene and then was saturated with hydrogen. As a result, the elemental composition of PE−PEP-6H is expected to be $[C_4D_6H_2]-[C_4H_8]$, or D:H = 0.60. This isotopic ratio was confirmed using a Rutherford backscattering measurement[23] that yielded D:H = 0.59 ± 0.02. This precise value will be needed in interpreting absolute intensity SANS data (see the following sections).

II-C. Rheological Measurements. Block copolymer rheology has been shown to be sensitive to morphology and orientation and therefore is quite useful in establishing phase behavior.[8,9,24-26] Dynamic shear moduli for each of the diblock copolymers listed in Table 1 were measured using two experimental procedures. The first is an isothermal frequency sweep that measures the frequency-dependent dynamic elastic, $G'(\omega)$, and loss $G''(\omega)$, moduli at constant temperature. The mechanical response of diblock copolymers to small oscillatory strains was shown earlier[8] to depend upon the phase state of the material at frequencies below a certain critical reduced frequency, $a_T\omega_c$, where a_T is the WLF shift factor. The second procedure, used to quantitatively determine T_{ODT}, is to slowly heat a specimen (0.1−1 °C/min) while monitoring G' and G'' at $\omega < \omega_c$. At the ODT the viscometric properties change discontinuously.[8,24]

Rheological experiments were conducted on the saturated diblock copolymers with Rheometrics RSA-II and RMS-800 dynamic mechanical spectrometers operated in the simple shear and cone and plate geometries, respectively. Specimens 0.6−1.0 mm thick were prepared by heating to 130 °C under vacuum (<0.1 Torr) while compressing between Teflon-covered plates. After cooling to room temperature, pieces were cut and mounted on the 12 mm × 16 mm × 0.5 mm shear sandwich fixture of the RSA-II or the 50 mm cone and plate (cone angle $\alpha = 0.04$ rad) of the RMS-800. The dynamic elastic (G') and loss (G'') shear moduli were determined for the diblock copolymer melts as a function of frequency ($0.002 \le \omega \le 100$ rad/s) and temperature ($10 \le T \le 200$ °C) while being subjected to a 2−5% strain amplitude.

PE−PEP and PE−PEE diblocks were only tested above 110 °C since the PE blocks are semicrystalline below 108 ± 2 °C. Sample temperature was controlled to ±1 °C with a thermally-controlled nitrogen gas purge. The RMS-800 was used primarily for obtaining isothermal frequency sweeps in generating "master plots" of the frequency- and temperature-dependent dynamic shear modulus data. The RSA-II was used in the fixed-frequency (isochronal) temperature ramp mode (heating 0.3−0.5 °C/min) for determining the order−disorder transitions.

II-D. SANS. Small-angle neutron scattering (SANS) experiments were performed at the 12-m SANS facility at Risø National Laboratory located in Roskilde, Denmark, and at the 30-m W.C. Koehler small-angle scattering facility located at Oak Ridge National Laboratory, Oak Ridge, TN. The Risø instrument was operated with $\lambda = 6.11$ and 6.20 Å wavelength neutrons ($\Delta\lambda/\lambda = 0.09$ and 0.18, respectively), pinhole collimation, and a sample-to-detector distance of 6 m. The Oak Ridge instrument was operated with $\lambda = 4.75$ Å wavelength neutrons ($\Delta\lambda/\lambda = 0.06$), pinhole collimation, and a sample-to-detector distance of 10 m. Each instrument employs an area detector. Sample temperature was controlled by mounting sealed-quartz sample cells (see below) in a thermally-controlled (±0.2 °C) copper block that contained a thin, neutron transparent, copper window.

Two types of SANS specimens were prepared: isotropic and anisotropic (i.e., shear-oriented). Isotropic samples of PE−PEP-6H, PEP−PEE-14H, and PE−PEE-8H were prepared by heating an appropriate amount of material above T_{ODT} (see the Results and Analysis section), cooling to room temperature, and mounting between 1-in.-diameter by 1/16-in.-thick quartz optical flats separated by a 0.125-cm annular aluminum spacer. A shear-oriented specimen of PE−PEP-3D was prepared in a shearing apparatus described elsewhere.[27] Square sheets of the ordered material (1-mm-thick by 25 cm^2) were subjected to a 100% strain amplitude oscillatory shear using a shear rate of $|\dot{\gamma}| = 0.02$ s^{-1} at 115 °C. This orientation procedure was conducted under nitrogen for 11 h, and then

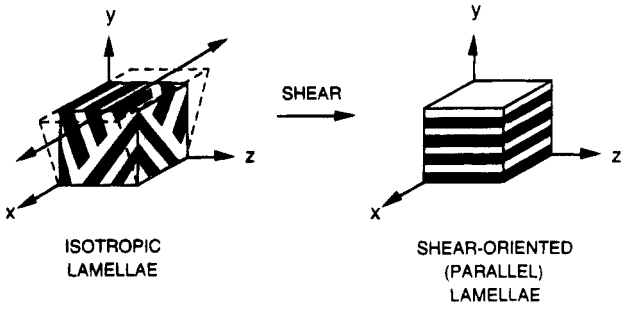

Figure 1. Illustration of shear orientation of isotropic (quenched) lamellae to the monodomain form where x−z, x, and y are the shear plane, the shear direction, and the shear gradient, respectively. Samples were cut and examined by SANS by directing the neutron beam along the x, y, and z directions.

the specimen was cooled to room temperature. Shear-oriented samples of PE−PEP-6H and PE−PEE-1H were prepared at 115 °C for 15−17 h using the same strain amplitude and $|\dot{\gamma}| = 0.08\ s^{-1}$. Three sets of SANS specimens were prepared with orientations established by the shearing coordinate system illustrated in Figure 1. Lamellar orientation in the $x-z$ plane was inspected by cutting a 1.0 cm × 1.0 cm piece from the semicrystalline oriented sheet and mounting it between optical quartz flats while maintaining sample orientation. The $y-z$ and $x-y$ planes were inspected by cutting and stacking 10 1 mm × 10 mm strips while maintaining the sample orientation. All of the quartz−sample assemblies were sealed in a purified argon drybox with epoxy to prevent degradation while testing.

Neutron scattering experiments on the anisotropic (shear-oriented) PE−PEP-3D sample and the isotropic PEP−PEE-14H and PE−PEE-8H samples were performed as a function of temperature on the Risø instrument. The shear-oriented PE−PEP-3D sample gave anisotropic diffraction patterns that are presented as relative intensity versus position in three-dimensional surface plots and two-dimensional contour plots. Isotropic and shear-oriented specimens of PE−PEP-6H and the shear-oriented PE−PEE-1H specimens were studied using the Oak Ridge instrument. The scattering data obtained for the isotropic PE−PEP-6H specimen near the ODT were corrected for detector sensitivity, background scattering, sample thickness, and transmission and placed on an absolute basis (±5%) using an irradiated aluminum (Al-4) secondary as described elsewhere.[28] The isotropic, two-dimensional data were reduced to the one-dimensional form of intensity versus $|\mathbf{q}| = q = 4\pi\lambda^{-1}\sin(\theta/2)$ where θ is the scattering angle, following established procedures.

III. Results and Analysis

III-A. Rheology. The dynamic shear moduli for each of the three polyolefin diblock copolymer systems in this study were examined using two experimental procedures. The first is an isochronal temperature ramp where the dynamic elastic (G') and loss (G'') shear moduli are measured while increasing the temperature at a fixed rate at constant strain amplitude and frequency. Proper choice of reduced frequency ($a_T\omega < a_T\omega_c'$ is the reduced frequency where the time−temperature superposition principle breaks down for the G' data) is required for observing the gross rheological changes associated with the order−disorder transition (ODT).[8] Figure 2 shows the temperature-dependent dynamic shear moduli of PE−PEP-6H obtained using 5% strain amplitude at a frequency of 0.2 rad/s while heating at 0.3 °C/min from 129 to 147 °C. The discontinuity in the G' data at 139 ± 1 °C signals the order−disorder transition. Order−disorder transition temperatures, T_{ODT}, for each polyolefin diblock copolymer listed in Table 1 were established using this rheological technique, except PEP−PEE-14H which was determined by

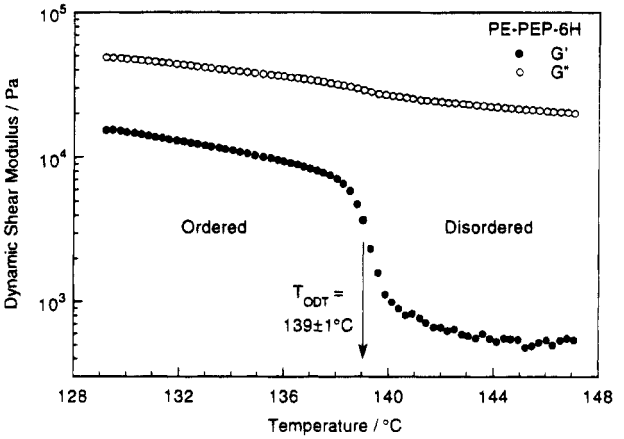

Figure 2. Temperature dependence of G' and G'' for sample PE−PEP-6H obtained while heating at 0.3 °C/min with a 5% strain amplitude and $\omega = 0.2$ rad/s. The discontinuity in G' at 139 ± 1 °C results from the order−disorder transition (ODT).

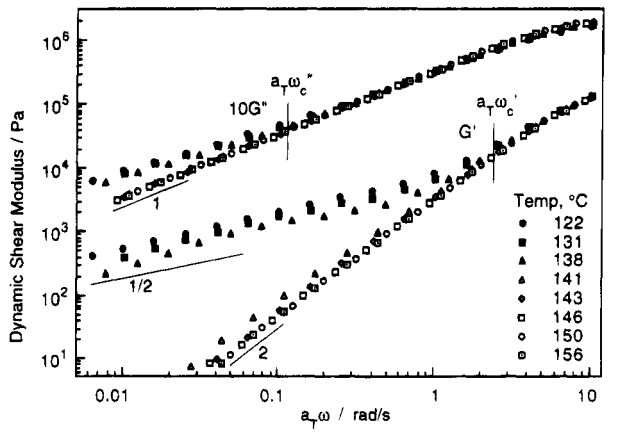

Figure 3. Reduced frequency plot for representative dynamic elastic (lower points) and loss (upper points) data obtained from sample PE−PEP-6H. Shift factors were determined by concurrently superimposing G' and G'' for $\omega > \omega_c'$ and $\omega > \omega_c''$, respectively, to the 122 °C data. The filled and open symbols correspond to the ordered and disordered states. Failure of time−temperature superposition in G' at 141 °C for $a_T\omega < a_T\omega_c'$ derives from fluctuation effects.

SANS (see below). Accuracy of these measurements is governed by the temperature control of the rheometer, typically ±1 °C, and by the heating rate; too high a heating rate leads to overestimation of T_{ODT} by several degrees or more. In all cases, the ODT temperatures determined rheologically agree within experimental error (±1 °C) with those obtained by small-angle neutron scattering (see below).

A reduced frequency plot, or so-called master plot, of isothermal frequency sweeps for sample PE−PEP-6H in the vicinity of T_{ODT} is given in Figure 3. Eight frequency sweeps were obtained at 3% strain amplitude with the 50-mm cone and plate fixtures of the RMS-800 and were shifted with respect to the 122 °C data using the high-frequency branches of the spectra. As described elsewhere,[8] superpositioning the data this way reveals the complex nature of the rheology of diblock copolymers near the ODT. In the ordered state (T = 122, 131, and 138 °C) PE−PEP-6H exhibits a frequency behavior similar to that observed with other lamellar systems[8,9] where $G' \approx G'' \sim \omega^{1/2}$. In the disordered state ($T > T_{ODT}$) a terminal viscoelastic limit, $G' \sim \omega^2$ and $G'' \sim \omega$, is reached at low frequencies. However, unlike our previous results on symmetric PEP−PEE diblock

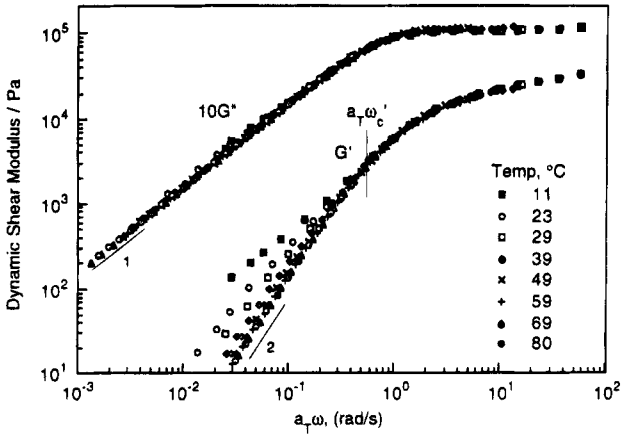

Figure 4. Dynamic shear modulus versus reduced frequency for sample PEP–PEE-14H. Shift factors were determined by concurrently superimposing G' and G'' for $\omega > \omega_c'$ and $\omega > \omega_c''$, respectively, to the 23 °C data. The filled and open symbols correspond to the ordered and disordered states. Failure of time–temperature superposition in G' above 23 °C for $a_T\omega < a_T\omega_c'$ derives from fluctuation effects.

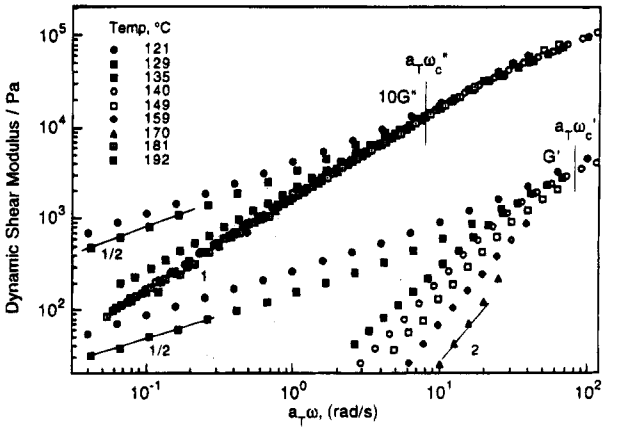

Figure 5. Reduced frequency plot for representative dynamic elastic and loss data obtained from sample PE–PEE-8H. Shift factors were determined by superimposing G'' data from $\omega > \omega_c''$ to the 121 °C data. The G' data have been shifted using the same a_T values. The filled and open symbols correspond to the ordered and disordered states. Failure of time–temperature superposition in G' above 135 °C for $a_T\omega < a_T\omega_c'$ derives from fluctuation effects.

copolymers,[5,6,8] where fluctuation effects were observed rheologically for $T - T_{ODT} \lesssim 50$ °C, in PE–PEP-6H this behavior is limited to $T - T_{ODT} < 7$ °C. Similar results were obtained for the other symmetric PE–PEP diblock copolymers but are not reproduced here for the sake of brevity.

The reduced frequency plot for PEP–PEE-14H, shown in Figure 4, was constructed by simultaneously shifting the G' and G'' data with respect to the 29 °C scan for $a_T\omega > a_T\omega_c'$. These data illustrate a practical limitation to the dynamic mechanical testing method for determining T_{ODT}. When $a_T\omega_c'$ is near or below the lowest measurable frequency (typically 0.01–0.001 rad/s for most commercial dynamic mechanical spectrometers) at T_{ODT}, the discontinuous drop in G' associated with the ODT is not observed. This limitation applied to PEP–PEE-14H and determination of T_{ODT} (16 ± 2 °C) required another technique (SANS, described below). Although the ODT for PEP–PEE-14H could not be readily observed rheologically, composition fluctuations in the disordered state are quite apparent in Figure 4 up to the 49 °C scan; above this temperature terminal viscoelastic behavior and full superposability are evident.

The reduced frequency plot of PE–PEE-8H, given in Figure 5, was constructed by shifting the nine frequency scans with respect to the G'' data at 121 °C. The critical elastic reduced frequency $a_T\omega_c'$ of this sample is higher than the upper frequency limit (100 rad/s) of the RMS-800 at these temperatures. This results from the relatively low molecular weight of PE–PEE-8H, compared to the other diblocks. However, it was reported earlier[8] that the critical *loss* reduced frequency, $a_T\omega_c''$, is about 10 times lower than a_{Tc}' in nearly symmetric PEP–PEE diblock copolymers so that the G'' data have a window of superposability for shifting; the same shift factors are used for plotting the G' data. Complex rheological behavior is also observed with PE–PEE-8H where $G' \approx G'' \sim \omega^{1/2}$ below T_{ODT} (136 ± 2 °C) and terminal viscoelastic behavior is approached at the higher test temperatures. As with the reduced frequency plots of PEP–PEE polymers (Figure 4 and refs 8 and 9) composition fluctuations in PE–PEE-8H are clearly evident in the G' data up to at least 170 °C, i.e., at least 34 °C above T_{ODT}. The temperature at which composition fluctuations disappear lies outside the rheological experimental range for sample PE–PEE-8H under linear viscoelastic conditions. This demonstrates another limitation of the rheological technique for characterizing composition fluctuations in low molecular weight diblock copolymers. Although G'' values are superposable, fluctuation effects on the dynamic loss data are too small to discriminate the crossover from nonsuperposability to superposability as demonstrated earlier.[8]

III-B. SANS: Oriented Lamellae. Three representative anisotropic neutron scattering patterns obtained at 111 °C from the shear-oriented (see Figure 1) PE–PEP-3D diblock copolymer are displayed in three-dimensional (3D) and two-dimensional (contour) form in Figure 6. The intensities depicted in the 3D plots are on the same relative linear scale, while the isointensity levels of the contour plots are linearly spaced at 10%, 30%, 50%, 70%, and 90% of the maximum intensity. These three scattering patterns are consistent with a "parallel" lamellae geometry, where the lamellar normals are directed perpendicular to the plane of shear[27] (see Figure 1). Higher-order reflections at $2q^*$ and $3q^*$, evident in $\mathbf{q}_x$–$\mathbf{q}_y$ and $\mathbf{q}_y$–$\mathbf{q}_z$ when inspected on a logarithmic scale (not shown here), further indicate that the lamellae were well developed. Recall that these diffraction patterns were obtained from a specimen that was sheared in the ordered melt state, cooled to room temperature, below the 108 °C PE melting temperature, and reheated to 111 °C. It is apparent from this result that crystallization does not disrupt the long-range order or orientation of the lamellae. Changes in the principal diffraction peaks in the $\mathbf{q}_x$–$\mathbf{q}_y$ plane with temperature are shown in Figure 7. The diffraction pattern at 111 °C is the same as that found in Figure 6c. As the temperature is increased to 153 °C the total intensity decreases (intensity magnification indicated in the lower left corner of each pattern) and the diffraction peaks spread azimuthally at fixed q^*. Nevertheless, the PE–PEP-3D sample is still ordered at 153 °C (T_{ODT} = 159 ± 1 °C, Table 1). This peak distortion is largely reversed by cooling, leading to nearly complete recovery of the 111 °C result. Disordering is apparent when the sample is heated above T_{ODT} to 163 °C; the diffraction pattern becomes azimuthally isotropic, and the intensity drops. After quenching back to 111 °C the

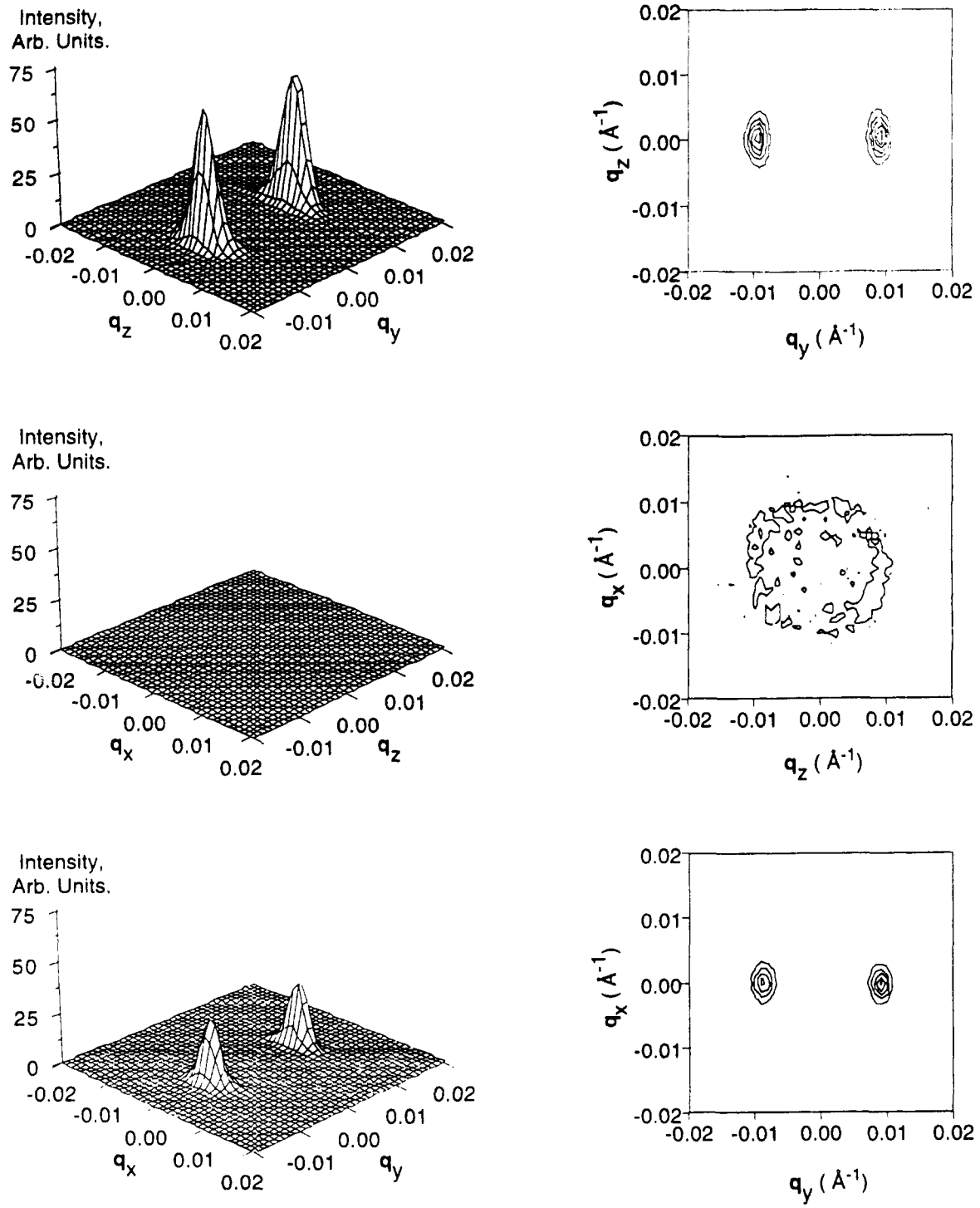

Figure 6. SANS patterns obtained from the shear-oriented PE–PEP-3D diblock copolymer at 111 °C. Coordinates are specified in Figure 1. The intensity scales in the three-dimensional surface plots are on a common relative linear scale, while the isointensity levels of the contour plots are linearly spaced at 10%, 30%, 50%, 70%, and 90% of the maximum intensity. The three scattering patterns confirm that the lamellae are oriented parallel to the shear plane as shown in Figure 1.

isotropic ring pattern persists as expected for randomly-oriented lamellae grown from the disordered state. The order–disorder transition temperature of PEP–PEE-14H was determined to be 16 ± 2 °C by locating the point where shear-induced anisotropy in the SANS pattern was lost upon heating.

The temperature dependence of the higher order reflections of the lamellar phase was investigated with a shear-oriented PE–PEP-6H specimen in the $\mathbf{q}_y$–$\mathbf{q}_z$ scattering plane. Intensity versus scattering wavevector $\mathbf{q}_y$ was obtained with a sector-average "pie slice" that spanned ±17.5° around the Bragg peak maximums obtained from the two-dimensional scattering patterns. Representative results are plotted for five temperatures between 110 and 138.7 °C (T_{ODT} = 139 ± 1 °C by rheology) in Figure 8. These clearly demonstrate the evolution of the composition profile as the ODT is approached. At 110 °C at least four Bragg reflections are present ($|\mathbf{q}_y|$ = 0.0111, 0.0216, 0.0320, and 0.0420 Å^{-1}) corresponding to q^*, $2q^*$, $3q^*$, and $4q^*$ as expected for the lamellae morphology (the peak positions were obtained by fitting a Lorentzian curve to each). More importantly, as PE–PEP-6H is heated toward the ODT, the number of Bragg reflections decrease to just one.

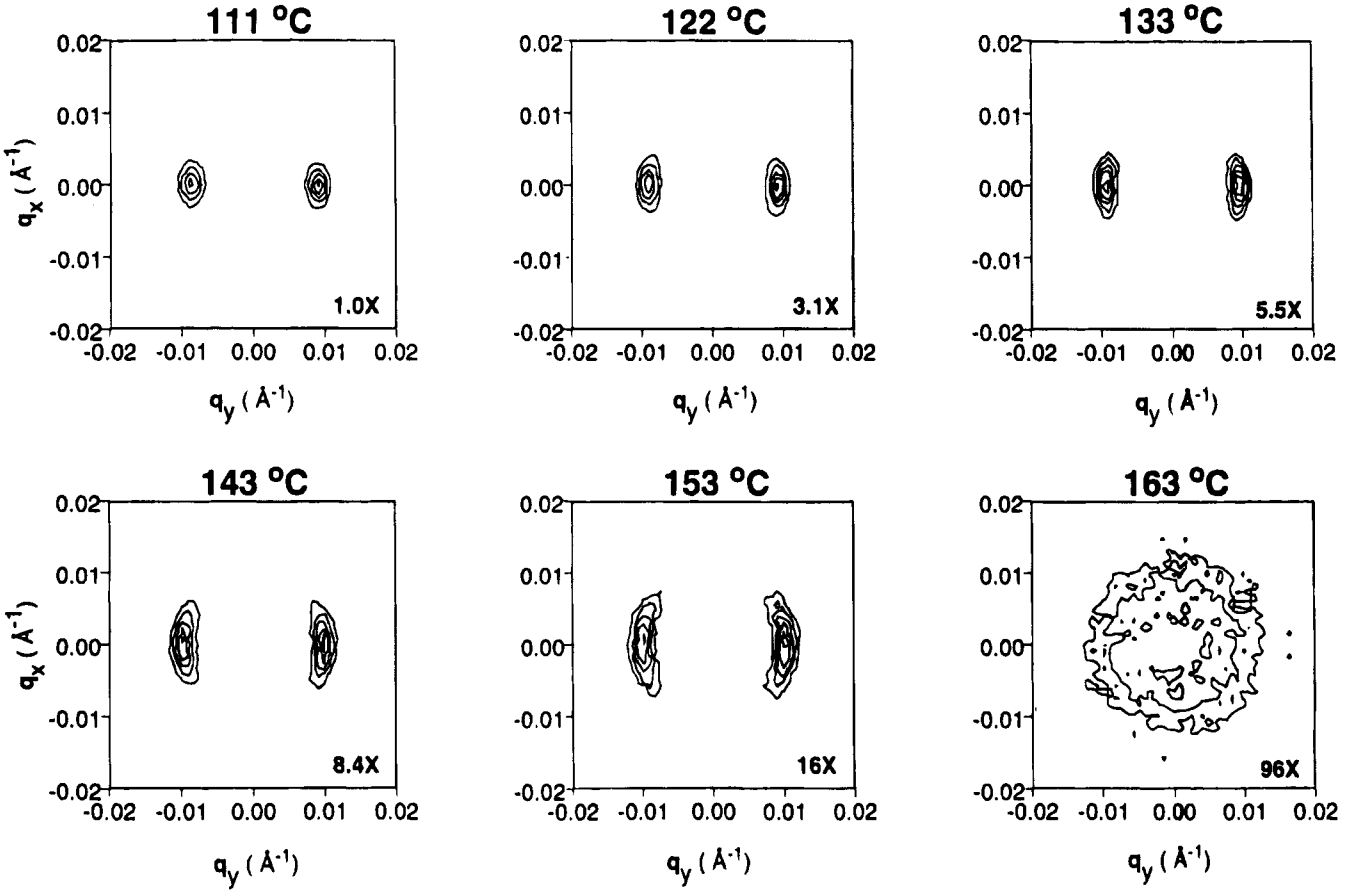

Figure 7. Evolution of the diffraction peaks of PE−PEP-3D in the $\mathbf{q}_x$−$\mathbf{q}_y$ scattering plane while heating. The total intensity decreases (intensity magnification indicated in the lower left corner of each pattern) and the diffraction peaks spread azimuthally at $|\mathbf{q}| = q^*$. Disorder is apparent at 163 °C (T_{ODT} = 159 ± 1 °C by rheology). Prior to disordering, the 111 °C pattern was recovered when cooled from 153 °C.

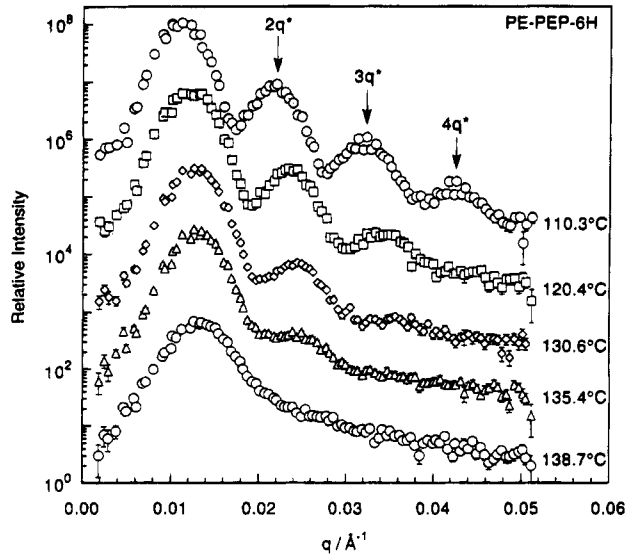

Figure 8. Relative intensity versus scattering wave vector obtained from shear-oriented PE−PEP-6H (f = 0.50) at several temperatures below T_{ODT} = 139 ± 1 °C. The steady decrease in the number and intensity of the higher order reflections as T_{ODT} is approached indicates a softening of the composition profile and a weakening of long-range correlations.

Notice also that the peak positions move to higher q as the ODT is approached and that the lowest two reflections are always in a ratio of q^* and $2q^*$ (e.g., at 135.4 °C the fitted peak positions are 0.01233 and 0.0231 ± 0.0002 Å^{-1}). This provides further evidence that the morphology remains lamellar up to the point of disordering.

The temperature dependence of the higher order reflections was also investigated with the shear-oriented PE−PEE-1H specimen in the $\mathbf{q}_y$−$\mathbf{q}_z$ scattering plane. Intensity versus $|\mathbf{q}_y|$, obtained using the same sector averaging procedure produced the results plotted for five temperatures between 124 and 179.8 °C (T_{ODT} = 182 ± 2 °C) in Figure 9. The positions of the peak intensities at 124 °C occur at about 0.025, 0.050, and 0.075 Å^{-1}, or q^*, $2q^*$, and $3q^*$, indicating that PE−PEE-1H is lamellar; as the ODT is approached the higher order reflections at $2q^*$ and $3q^*$ also decay, consistent with a direct transition from lamellae to the disordered state.

III-C. SANS: Isotropic. Examples of the $I(q)$ scattering profile in absolute intensity units for PE−PEP-6H in the disordered state at 140.7 and 159.9 °C (±0.2 °C) are depicted in Figure 10a. We have attempted to fit the data with the Leibler[2] structure factor, $S(q)$.

$$I(q) = (b_A - b_B)^2 v^{-1} S(q) \tag{5}$$

$$S(q)^{-1} = N^{-1}F(x,f) - 2\chi_{eff} \tag{6}$$

$$x = q^2 R_g^{\,2} = q^2(a_A^{\,2}N_A + a_B^{\,2}N_B)/6 \tag{7}$$

where b_A and b_B are the segment scattering lengths, v is the segment volume, and $F(x,f)$ is the bare correlation function for a melt of Gaussian diblock copolymer coils. In using eqs 5−7, we have made corrections for instrument smearing[29] and polydispersity.[30] Only two pa-

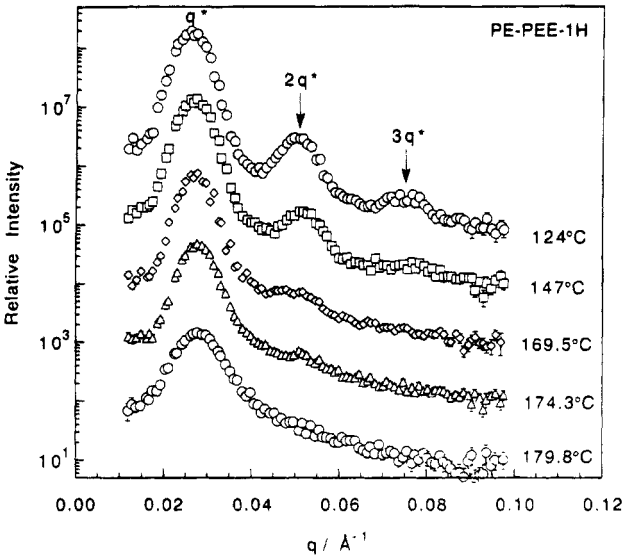

Figure 9. Relative intensity versus scattering wave vector obtained from shear-oriented PE–PEE-1H ($f = 0.48$) at several temperatures below $T_{ODT} = 182 \pm 2$ °C. This behavior is similar to that shown in Figure 8.

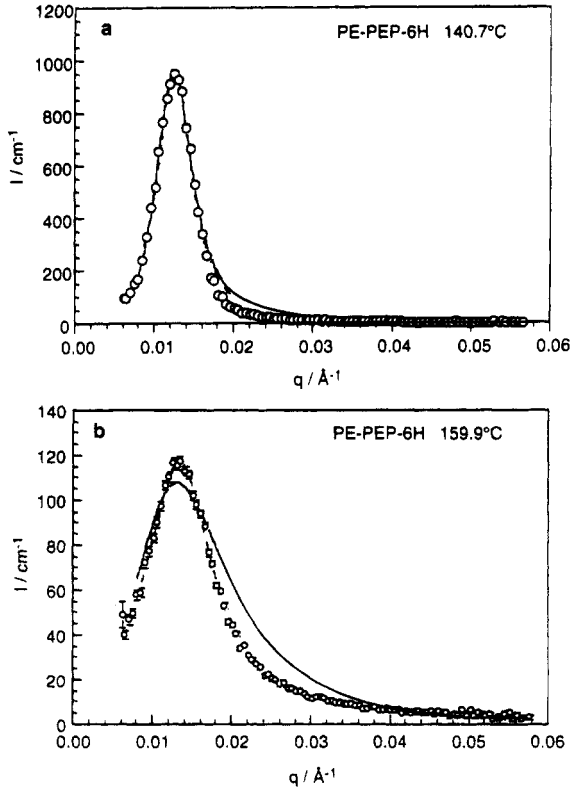

Figure 10. Absolute intensity SANS results for disordered sample PE–PEP-6H at (a) 140.7 and (b) 159.9 °C. Solid curves are instrument smeared, and polydispersity corrected fits of eqs 5 and 6 where χ_{eff} and $\langle a \rangle$ have been varied. Dashed curves are Lorenzian fits (eq 10).

rameters, χ_{eff} and the effective statistical segment length $\langle a \rangle$,

$$\langle a \rangle^2 = f_A a_A^2 + (1 - f_A) a_B^2 \tag{8}$$

were adjusted in modeling the SANS data. The contrast factor, N, N_w/N_n, and f_A are known with fair precision for PE–PEP-6H, as well as the instrument resolution function. In fitting eq 6 we have assumed $a_{PE} = 1.22 a_{PEP}$ (see below). Increasing $\langle a \rangle$ shifts q^* to lower values, while increasing χ_{eff} raises $I(q^*)$, thereby decreasing the full width at half-maximum (fwhm) of the scattering peak. We could not successfully fit the theoretical function $S(q)$ over the entire q-range within the uncertainty in the molecular parameters. The solid curves shown in Figure 10 were obtained by optimizing the fit around q^* where $\langle a \rangle \cong 7.54$ and 7.20 Å at 140.7 and 159.9 °C, respectively. Although the peak data are well accounted for, particularly as $T \rightarrow T_{ODT}$, the intensities at $q > q^*$ are systematically overpredicted by the theoretical structure factor. These differences would not be readily apparent in the absence of absolute intensity calibration since one additional adjustable parameter (e.g., the absolute intensity) would enable a quantitative adjustment of the fwhm. A possible source for these discrepancies may be compressibility (density fluctuation) effects which have been modeled by Tang and Freed.[31] Unfortunately, the associated structure factor relies on additional parameters that are not directly available for our materials, making a quantitative evaluation impossible. However, we note that the qualitative effect of adding a finite compressibility is to reduce the overall scattering intensity around q^*, which would improve the fit to our experimental results. We intend to design future experiments to test this important concept.

Because scattering at $q > q^*$ is dominated by correlations less than a radius of gyration in size, the intensity in this regime is dominated by the amount of local mixing, and the conformation, of the chain segments. In the limit $q \gg q^*$,

$$S(q) \cong \frac{12\phi(1-\phi)}{q^2\langle a \rangle^2} \tag{9}$$

where ϕ is the local composition ($\phi = f$ in the mean-field limit). Thus, the lower than predicted intensity on the high q side of the peak could be related to local demixing (i.e., $\phi < f$), or to a larger-than-anticipated $\langle a \rangle$. The high-q scattering regime can be fitted with eq 9 to determine ϕ if $\langle a \rangle$ is known or $\langle a \rangle$ if ϕ is known. In fact, the high-q portions of the PE–PEP-6H SANS patterns are quantitatively accounted for by the Gaussian scaling anticipated by eqs 5 and 9, $I(q) \sim q^{-2}$, as shown by the solid curves in Figure 11. If we assume unperturbed block coil dimensions [i.e., $\langle a \rangle^2 = 1/2(a_{PE}^2 + a_{PEP}^2)$ with $a_{PE}(140\ °C) = 8.2$ Å, $a_{PEP}(140\ °C) = 6.7$, and $\partial \ln a_{PE}/\partial T = \partial \ln a_{PEP}/\partial T = -0.58 \times 10^{-3}$],[31] then $\langle a \rangle_{PE-PEP} = 7.8$ Å at 140 °C and 7.7 Å at 159 °C, close to what we extracted from the peak fits. With these values the fitted curves in Figure 11 yield $\phi \cong 0.77$ at both temperatures. Alternatively, fixing $\phi = f = 1/2$ leads to $\langle a \rangle \cong 9.2$ Å, implying that the chains are either stretched or distributed nonrandomly. In fact, this value of $\langle a \rangle$ is considerably larger than that extracted from the peak position. These results indicate a significant deviation from the unperturbed and randomly distributed Gaussian coil behavior assumed in the mean-field theory.[2]

Because of these difficulties in fitting the PE–PEP-6H SANS data using the corrected Leibler structure factor, the peak position, q^*, and peak intensity, $I(q^*)$, for each temperature were determined by fitting a Lorentzian function,

$$I(q) = \frac{I(q^*)}{1 + (q - q^*)^2(\Delta q)^{-2}} \tag{10}$$

where Δq represents the full width at half-maximum

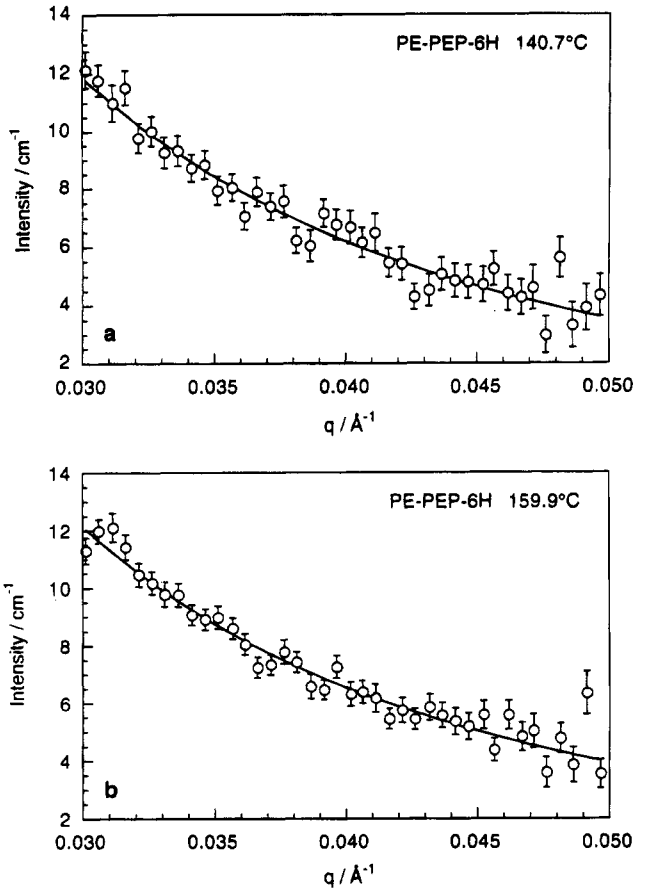

Figure 11. Absolute intensity SANS results with $q \gg q^*$ for sample PE–PEP-6H ($f = 0.50$) at (a) 140.7 and (b) 159.9 °C in the disordered state. The solid curve represents eq 9. If the local composition is assumed to be stoichiometric, then $\langle a \rangle \cong$ 7.7 or 7.8 Å, while fixing $\langle a \rangle$ at the unperturbed Gaussian coil value leads to $\phi \cong 0.77$.

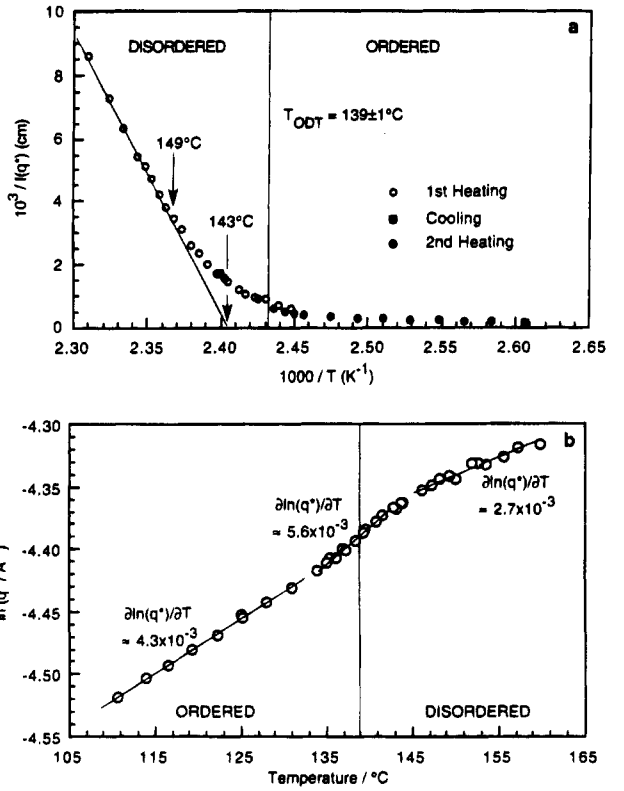

Figure 12. Temperature dependence of (a) inverse peak scattering intensity, $I(q^*)^{-1}$, and (b) peak position, q^*, for isotropic sample PE–PEP-6H. The linearity in $I(q^*)^{-1}$ versus T^{-1} above 149 °C is consistent with the mean-field treatment, while the nonlinearity below 149 °C results from composition fluctuations. A stretching transition is indicated by the change in $\partial \ln (q^*)/\partial T$, at about 145 °C. In each of the three regimes, the temperature dependence of q^* greatly exceeds that of the unperturbed coils.

(fwhm) of the peak. The peak position and inverse peak intensity are plotted versus temperature and inverse temperature in parts a and b of Figure 12, respectively. Measurements obtained between 110 and 160 °C while heating, cooling, and reheating the diblock copolymer melt are reproducible. According to Leibler's mean-field theory, the stability limit T_s is established by the point where $I(q^*)$ diverges, or $I^{-1}(q^*) = 0$. For PE–PEP-6H extrapolation of the linear, high-temperature portion of $I^{-1}(q^*)$ versus T^{-1} yields $T_s = 143$ °C. However, at $T_x = 149$ °C the inverse intensity curves away from linearity. Without the benefit of rheology (Figure 2) and the SANS measurements on oriented samples (Figure 6), this might have been misinterpreted as the ODT (see below). Instead, we will show that this curvature in $I^{-1}(q^*)$ derives from isotropic fluctuations (see section IV-C).

The peak position, q^*, increases with temperature as shown in Figure 12b. Three different dependencies of $\ln q^*$ on temperature are observed: $\partial \ln(q^*)/\partial T \approx 4.3 \times 10^{-3}$ below approximately 130 °C; $\partial \ln(q^*)/\partial T \approx 5.6 \times 10^{-3}$ between 135 and 145 °C; $\partial \ln(q^*)/\partial T \approx 2.7 \times 10^{-3}$ above 145 °C. These values cannot be accounted for by the base temperature dependence of the radius-of-gyration $\partial \ln(R_g)/\partial T = \partial \ln \langle a \rangle/\partial T = -0.58 \times 10^{-4}$, which is about 10 and 4 times smaller than the observed temperature dependencies of q^*. This implies that mechanisms other than simple coil thermal expansion are operative near the ODT in PE–PEP-6H and indicates that the molecules are either stretched beyond their Gaussian conformation or distributed nonrandomly.

The isotropic, azimuthally averaged scattering profiles for PEP–PEE-14H (disordered state) were fitted for peak position and intensity using the same procedures described for PE–PEP-6H based on eqs 5–7. Because these data were not calibrated to absolute intensity, we cannot comment on the detailed nature of fits to the Leibler structure factor. Figure 13a depicts the temperature-dependent SANS peak intensity in the vicinity of T_{ODT} as $I(q^*)^{-1}$ versus T^{-1} for this sample. Initial measurements were obtained by heating from room temperature to about 130 °C in 40 °C steps. The sample was cooled back to room temperature and more measurements were obtained while heating to about 150 °C in 6 °C steps and finally while cooling to ensure reproducibility. Two important results emerge from these data. First, the $I(q^*)^{-1}$ data are linear in T^{-1} at temperatures higher than $T_x = 90$ °C, in agreement with the expected mean-field form. Second, the $I(q^*)^{-1}$ data deviate from linearity below this point due to composition fluctuations. The temperature dependence of the peak position is plotted in Figure 13b as $\ln q^*$ versus T. Data points obtained while heating and cooling are the same as in Figure 13a. Two different regimes in the dependence of $\ln q^*$ on temperature are observed; $\partial \ln(q^*)/\partial T \approx 1.3 \times 10^{-3}$ below approximately 60 °C and $\partial \ln(q^*)/\partial T \approx 0.4 \times 10^{-3}$ above 80 °C. These values are smaller than those determined for PE–PEP-6H, due in large part to a positive PEE coil thermal expansivity, $\partial \ln a_{PEE}/\partial T \cong 0.2 \times 10^{-3}$.[32]

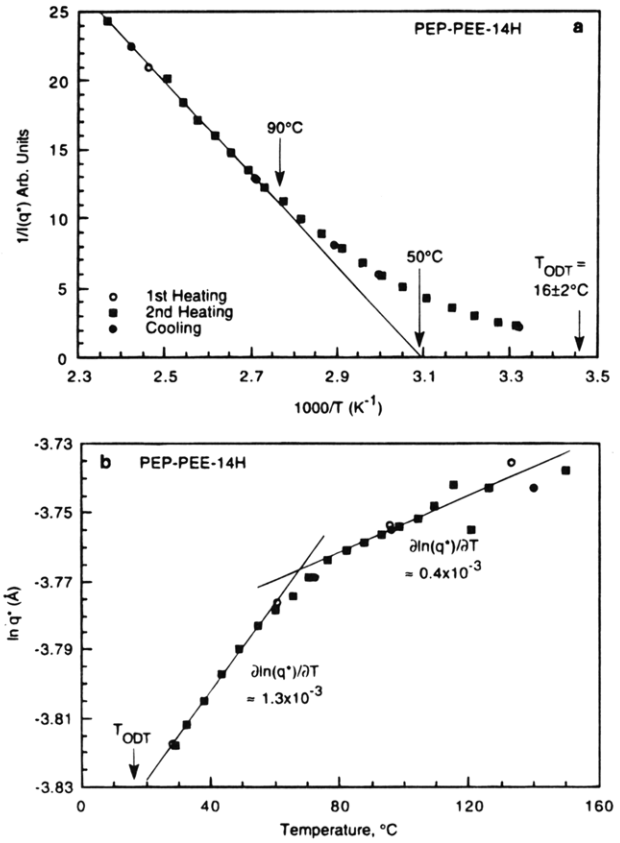

Figure 13. Temperature dependence of (a) inverse peak scattering intensity, $I(q^*)^{-1}$, and (b) peak position, q^*, for isotropic sample PEP–PEE-14H. $I(q^*)^{-1}$ is linear with T^{-1} above 90 °C, in agreement with the mean-field treatment for disordered diblock copolymers. Nonlinearity below 90 °C results from composition fluctuations. A chain stretching transition is indicated by the change in $\partial \ln(q^*)/\partial T$, at about 65 °C, analogous to that found in Figure 12.

Analogous SANS measurements for PE–PEE-8H in the disordered state are summarized in Figure 14. $I(q^*)^{-1}$ is plotted versus T^{-1} in Figure 14a. A crossover from linear to nonlinear behavior occurs at $T_x \cong 210$ °C, about 75 °C above T_{ODT}. Extrapolation of the linear region intercepts $I(q^*)^{-1} = 0$ at about 179 °C. The temperature dependence of the peak position is shown in Figure 14 as ln q^* versus T. Two different dependencies of ln q^* on temperature can be extracted, $\partial \ln(q^*)/\partial T \approx 1.2 \times 10^{-3}$ below approximately 179 °C and $\partial \ln(q^*)\partial T \approx 0.6 \times 10^{-3}$ above 210 °C, similar to what was found for PEP–PEE-14H.

IV. Discussion

IV-A. Lamellar State. A lamellar-to-disorder transition occurs in all the polyolefin diblock copolymers we examined. The dynamic mechanical behavior of each polyolefin diblock copolymer in the ordered lamellar phase is nonterminal with $G' \approx G'' \sim \omega^{1/2}$ at low frequencies, where $a_T\omega_c' \approx 10(a_T\omega_c'')$. A "softening" in the reduced G' traces occurs as the ODT is approached. This effect is most obvious in the dynamic mechanical data for PE–PEP-6H and PE–PEE-8H (Figure 3 and 5, respectively) where G' decreases by up to a factor of 2 at low reduced frequencies as T is increased to T_{ODT}. Such lamellar softening near the ODT can be attributed to composition fluctuations and weakening of the composition profile, which degrades the integrity of the lamellae. In a recent report, Amundson and Helfand[33]

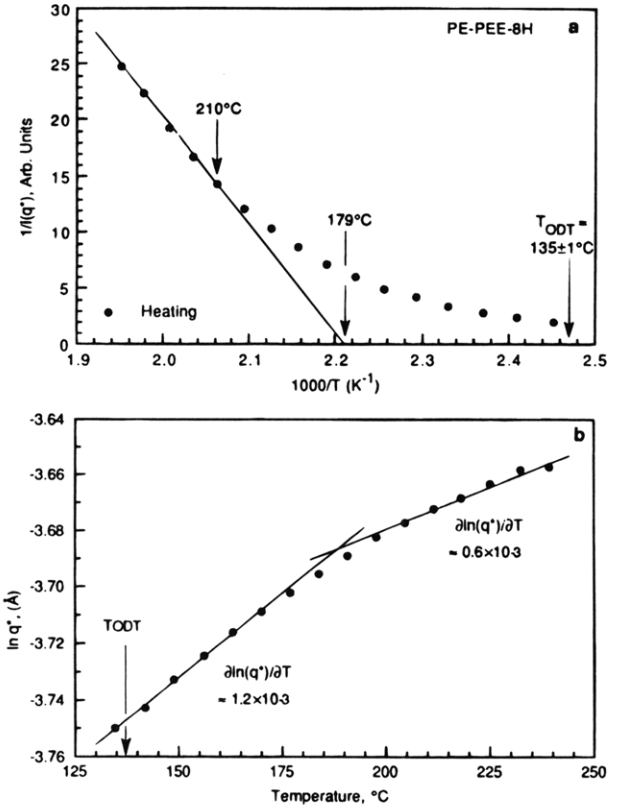

Figure 14. Temperature dependence of (a) inverse peak scattering intensity, $I(q^*)^{-1}$, and (b) peak position, q^*, for isotropic sample PE–PEE-8H. A mean field to non-mean-field transition is indicated by a departure from linearity at 210 °C in $I^{-1}(q^*)$. This is accompanied by a change in the temperature dependence of q^*, similar to what is found in Figures 12 and 13.

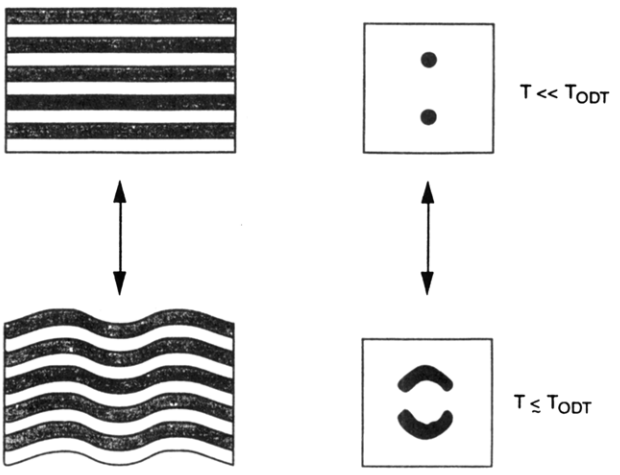

Figure 15. Illustration of lamellar deformation by rippling, and the associated changes in scattering patterns, as $T \rightarrow T_{ODT}$.

calculated the quasi-state mechanical properties of the lamellar diblock copolymer microstructure near the ODT in terms of a layer compressibility and an elastic splay constant. They incorporated the simplified fluctuation-corrected form of the diblock copolymer free energy provided by Fredrickson and Binder[34] into the phenomenological form of the distortion energy of a smectic A phase, as proposed by de Gennes.[35] Their calculations suggest that lamellae softening due to fluctuations makes the microstructure more susceptible to various distortions near the ODT, such as the formation of edge dislocations and "rippling", or "splay" distortions, as shown in Figure 15.

Neutron diffraction patterns from oriented lamellae (e.g., Figures 6–9) maintain equitorial reflections as the samples are heated to the ODT. However, arcing of the principal diffraction spots at $|\mathbf{q}| = q^*$ (e.g., the 10% isointensity contour increased from ±20° at 111 °C to θ = ±42° at 153 °C in Figure 7) indicates that the lamellae become distorted. Amundson and Helfand[33] calculated that fluctuations in the composition profile make the lamellae more susceptible to distortions as T_{ODT} is approached. Of the several types of distortions they investigated (movement of edge dislocations, nucleation and growth of undistorted ordered and disordered regions, and rippling), only rippling (see Figure 15) appears to be thermally reversible under static conditions. Therefore, we interpret the diffraction spot "arcing" found in Figure 7 as evidence of rippling and associate this mode of deformation with the loss of mechanical integrity noted above.

As the ODT is approached, the composition profile becomes increasingly sinusoidal[36] and the degree of long-range order decreases. Both factors contribute to a reduction in the number and intensity of the higher order reflections as seen in Figures 8 and 9. This overall softening of the ordered state permits the stretched coils to recover a larger and larger degree of their unperturbed conformation, leading to the largest value of $\partial \ln(q^*)/\partial T$ found over the entire range of χN (see Figure 12). This behavior persists right through the ODT, with $q^*(T)$ unaffected by the loss of long-ranged order. From this we can conclude that the local composition gradients are not strongly correlated with the degree of long-ranged order (also see ref 6).

These results conclusively demonstrate that the lamellar phase makes direct contact with the disordered state in symmetric diblock copolymers. We find no evidence for a hexagonal phase adjacent to the ODT,[37] although layered hexagonal phases have been observed between lamellae and cylinders in asymmetric ($f \neq 1/2$) polyolefin diblocks.[38]

IV-B. Order to Disorder. Perhaps the most important thermodynamic feature in block copolymer phase behavior is the order–disorder transition (ODT) which separates regions characterized by broken translational and orientational symmetry from the isotropic state. This first-order phase transition can be identified in a variety of ways; however, owing to the weak fluctuation driven nature of the ODT, the accuracy of its assignment may be compromised by certain experimental limitations as described here.

Perhaps the easiest method for determining T_{ODT} is via a low-frequency isochronal viscoelastic measurement as shown in Figure 2 and elsewhere.[5,6,8,24] Provided the heating rate is sufficiently slow and $a_T\omega < a_T\omega_c$, this technique yields a transition temperature within the accuracy of the instrument temperature resolution (approximately 1–2 °C). Order and disorder are also reflected in the frequency domain through isothermal measurements as shown in Figures 3–5. Here the effects of fluctuations in the disorder state, $T > T_{ODT}$, could be misinterpreted as evidence of order, leading to estimated transition temperatures that are significantly higher than the actual value. In fact, if we relied on the temperature where a departure from time–temperature superposition first fails as the criterion for T_{ODT},[39] then our assignments (Table 1) would increase by roughly 6, 40, and 50 °C for the PE–PEP, PEP–PEE, and PE–PEE polymers, respectively. Direct evidence of symmetry breaking as the material passes through the ODT is provided by scattering data from oriented specimens (see Figure 7), which corroborates these assignments.

The ODT can also be identified using small-angle scattering measurements, with either macroscopically isotropic or oriented specimens (see Figure 7). Both the peak intensity and shape, but not q^*, are affected by the degree of long-ranged order. A convenient approach is to monitor the width of the principal (q^*) reflection as a function of temperature in an isotropic sample.[4,40] Heating through the first-order ODT leads to a discontinuous broadening of the peak since the correlation length drops precipitously with disordering. However, this method is not very well suited for SANS since the limited instrument resolution (primarily the wavelength distribution) smears these differences almost beyond recognition.[6] Changes in the peak intensity $I(q^*)$ can also be correlated with a phase transition,[6] although this is probably the least reliable method for establishing T_{ODT}. As we discuss in the following section fluctuation effects also influence $I(q^*)$, and these should not be misinterpreted as evidence for the ODT. We believe that prior reports[39–41] that associate the ODT with departure from linearity in a plot of $I^{-1}(q^*)$ versus T^{-1} are in error.

Finally, order and disorder is often associated with the occurrence or absence, respectively, of higher order reflections.[40,42,43] This is also a rather crude gauge of the phase state in block copolymer melts owing to the very weak first-order character of the ODT. While the higher order reflections do disappear in the vicinity of T_{ODT} (see Figures 8 and 9), it would be difficult to use this criterion with much precision. Moreover, in the limit of very high molecular weight, where the composition profile approaches true sinusoidal form, only one reflection will remain, even well below T_{ODT}.

Examination of the ODT temperatures listed in Table 1 reveals the expected correlation between N and T_{ODT}. These values have been used to estimate $\chi(T)$ as detailed in the Appendix (also see below). Isotope substitution has a very modest impact on T_{ODT} as evidenced by a comparison of samples PE–PEP-2H and PE–PEP-6H. These materials have nearly identical degrees of polymerization and the largest isotopic difference used in this study. Nevertheless, T_{ODT} is the same for both materials. This result is not surprising. The pure isotope effect (i.e., with complete substitution) in saturated hydrocarbon homopolymers at 105 °C is $\chi_{HD} \approx 6 \times 10^{-4}$ based on a four-carbon repeat unit.[44,45] Partial labeling, as was used in the present study, will reduce this further[45] so that the estimated magnitude of the isotopic contribution to χ will be roughly 5% in PE–PEP-6H, 2% in PEP–PEE-14H, and 1% in PE–PEE-8H. These translate into a maximum variation in T_{ODT} of roughly 5 °C.

IV-C. Disordered State. Composition Fluctuations. Earlier studies by our group[5,6,46] demonstrated that the disordered region just above T_{ODT} is characterized by large-amplitude isotropic composition fluctuations. The magnitude of variations in the local composition

$$\psi(\mathbf{x}) = \phi(\mathbf{x}) - f \tag{11}$$

can be estimated using the disordered phase structure factor[47]

$$\langle|\psi(\mathbf{x})|^2\rangle = V\int \frac{d\mathbf{q}}{(2\pi)^3} S_0(\mathbf{q}) \tag{12}$$

where $V = Nv$ is the overall chain volume.

$$S_0(\mathbf{q}) \cong c^2[r_0 + 6R_g^2(\mathbf{q} - q^*)^2] \tag{13}$$

where the renormalized inverse susceptibility is given by

$$r_0 = \tau + \frac{d\lambda}{(r_0\bar{N})^{1/2}} \tag{14}$$

where

$$\tau = \frac{2}{c^2}[(\chi N)_s - \chi N] \tag{15}$$

$(\chi N)_s$ is the mean-field stability condition, $d = 3(q^*R_g)^2/2\pi$, and c and λ are constants that have been tabulated in ref 3; for $f = 1/2$, $d = 1.81$, $c = 1.10$, and $\lambda = 106.2$. Integration reduces eq 13 to

$$\langle|\psi(\mathbf{x})|^2\rangle = \frac{2d}{c^2(r_0\bar{N})^{1/2}} \tag{16}$$

Thus, in the mean-field limit ($\bar{N} \to \infty$) $\langle|\psi(\mathbf{x})|^2\rangle \to 0$ and the Leibler result is recovered. At the ODT ($f = 1/2$)[3]

$$r_0 = 0.201(d\lambda)^{2/3}\bar{N}^{-1/3} \tag{17}$$

and substitution of this expression into eq 16 yields

$$\langle|\psi(\mathbf{x})|^2\rangle = 1.16\bar{N}^{-1/3} \tag{18}$$

or the root-mean-square result

$$\langle|\psi(\mathbf{x})|^2\rangle^{1/2} = 1.08\bar{N}^{-1/6} \tag{19}$$

Using $\bar{N} = 2.8 \times 10^4$ (PE−PEP) and $\bar{N} = 4 \times 10^3$ (PEP−PEE and PE−PEE) (see Table 2) we obtain root-mean-square composition fluctuation amplitudes of 0.20 and 0.27, respectively. These values are consistent with that estimated from Figure 11, $\phi - f \approx 0.27$ (see above). We should emphasize that such large-amplitude critical-like fluctuations are a consequence of ordering at finite q^*. As $q^* \to 0$ (e.g., in Ising-like systems, such as binary mixtures) the solution of eq 12 leads to infinitesimally small fluctuation amplitudes, i.e., $\langle|\psi(\mathbf{x})|^2\rangle <<< 1$.

In this work we have identified a crossover to mean-field-like behavior around $T = T_x$ as shown in Figures 12−14. The difference $T_x - T_{ODT}$ can be used to gauge the extent of the fluctuation regime (see below); it spans about 75 °C for both PEP−PEE-14H and PE−PEE-8H and 10 °C for PE−PEP-6H (Table 2). Because block copolymer phase behavior is governed by the combined parameter χN, a proper comparison of these results requires a knowledge of $\chi(T)$. Our method for determining $\chi(T)$ for each polyolefin diblock, based on the BLFH theory, is given in the Appendix. The results

$$\chi_{PE-PEP-6H} = 10.25/T - 0.019$$

$$\chi_{PEP-PEE-14H} = 4.46/T + 0.0015$$

$$\chi_{PE-PEE-8H} = 15.0/T - 0.0055$$

were used to calculate the $(\chi N)_x$ and $(\chi N)_{ODT}$ values listed in Table 2; also provided are values of $\bar{N}$ determined at T_{ODT}.

Comparison of the $\bar{N}$ values listed in Table 2 reveals that PE−PEP-6H ($\bar{N} = 2.8 \times 10^4$) has the largest of the three listed, and therefore it should exhibit more mean-field-like character than either PEP−PEE-14H ($\bar{N} = 0.43 \times 10^4$) or PE−PEE-8H ($\bar{N} = 0.33 \times 10^4$). Note that these values are much larger than N_n because $\bar{N}$ depends strongly on the statistical segment length (see the Appendix). Values of $(\chi N)_{ODT}$ calculated with the fluctuation theory range from about 11.9 for PE−PEP-6H to about 13.3 for either PEP−PEE-14H or PE−PEE-8H. Hence, composition fluctuations in PE−PEP-6H are expected to be confined to a narrower region near the ODT than in either PEP−PEE-14H or PE−PEE-8H. In fact, the difference

Table 2. Characteristic Transition Points

diblock	$10^4\bar{N}^a$	T_{ODT}, °C	$(\chi N)_{ODT}{}^b$	T_x,[c] °C	$(\chi N)_x{}^d$
PE−PEP−6H	2.77	139 ± 1	11.9	149 ± 2	10.8 ± 0.2
PEP−PEE−14H	0.427	16 ± 2	13.4	90 ± 9	10.9 ± 2
PE−PEE−8H	0.325	136 ± 2	13.3	210 ± 12	10.9 ± 0.3

[a] $\bar{N} = N_n a^6 v^{-2}$ evaluated at the order−disorder transition. [b] Equations A-1 and A-2. [c] Identified in Figures 12−14. [d] χ evaluated at T_x using eqs A-9−A-11.

$$\Delta(\chi N) = (\chi N)_{ODT} - (\chi N)_x \tag{20}$$

is smaller for PE−PEP ($\Delta(\chi N) \cong 1.1$) than for either PEP−PEE-14H or PE−PEE-8H ($\Delta(\chi N) \cong 2.4$) (see Table 2), consistent with the prediction (eq 1) that the region over which composition fluctuations matter scales as $\bar{N}^{-1/3}$. This $O(\bar{N}^{-1/3})$ correction to the mean-field theory represents a type of Ginzburg parameter[48] that identifies where the crossover from mean-field to fluctuation behavior occurs. Consistent with this reasoning and eq 1, we find that $(\chi N)_x = 10.8 \pm 0.2$ (Table 2) for each of the three polyolefin diblock copolymers.

In a separate publication[47] we have shown that a hydrodynamic (shear) field also reduces $\Delta(\chi N)$, by suppressing fluctuations, thereby increasing T_{ODT}. The theory that describes these results was developed by Cates and co-workers[49,50] beginning with the static two-point correlation function given in eqs 13−15. They showed that, as the shear rate, $\dot{\gamma}$, is increased beyond the fluctuation time $1/\dot{\gamma}^*$, the mean-field result, $(\chi N)_{ODT} = 10.5$, is recovered; i.e., $\Delta(\chi N)_x \to 0$, analogous to the $\bar{N} \to \infty$ limit. Moreover, the presence of a symmetry breaking field leads to the recovery of a stability limit ($T_s = -\infty$ in the static case[3]) that merges with the ODT as $\dot{\gamma} \to \infty$. Our dynamic shear/SANS experiments[46] have confirmed this theoretical picture, lending strong support to the fluctuation picture originally proposed by Brazovskii[16] and complimenting the results presented here.

Conformational Effects. Changes in the local composition field near T_x, manifested in $I^{-1}(q^*)$ and the low-frequency rheology, are accompanied by distinct variations in the composition modulation period $d = 2\pi/q^*$. Before focusing on $(\chi N)_{ODT}$ and $(\chi N)_x$, we will briefly review the broader picture in the limits of weak and strong segregation. For $\chi N \to 0$ (weak segregation limit, WSL) and $\chi N \gg (\chi N)_{ODT}$ (strong segregation limit, SSL) d can be directly related to the conformational states of individual polymer blocks. In the WSL Leibler[2] has shown that $d \sim N^{1/2}$ while SSL theories[51,52] anticipate $d \sim N^{2/3}$, where the constants of proportionality depend on the statistical segment length a.

As the ODT is approached, fluctuation effects in the disordered state, and a finite interfacial thickness in the ordered state, complicate these simple limiting scaling predictions. In an earlier publication[53] we showed that a series of nearly symmetric PEP−PEE diblock copoly-

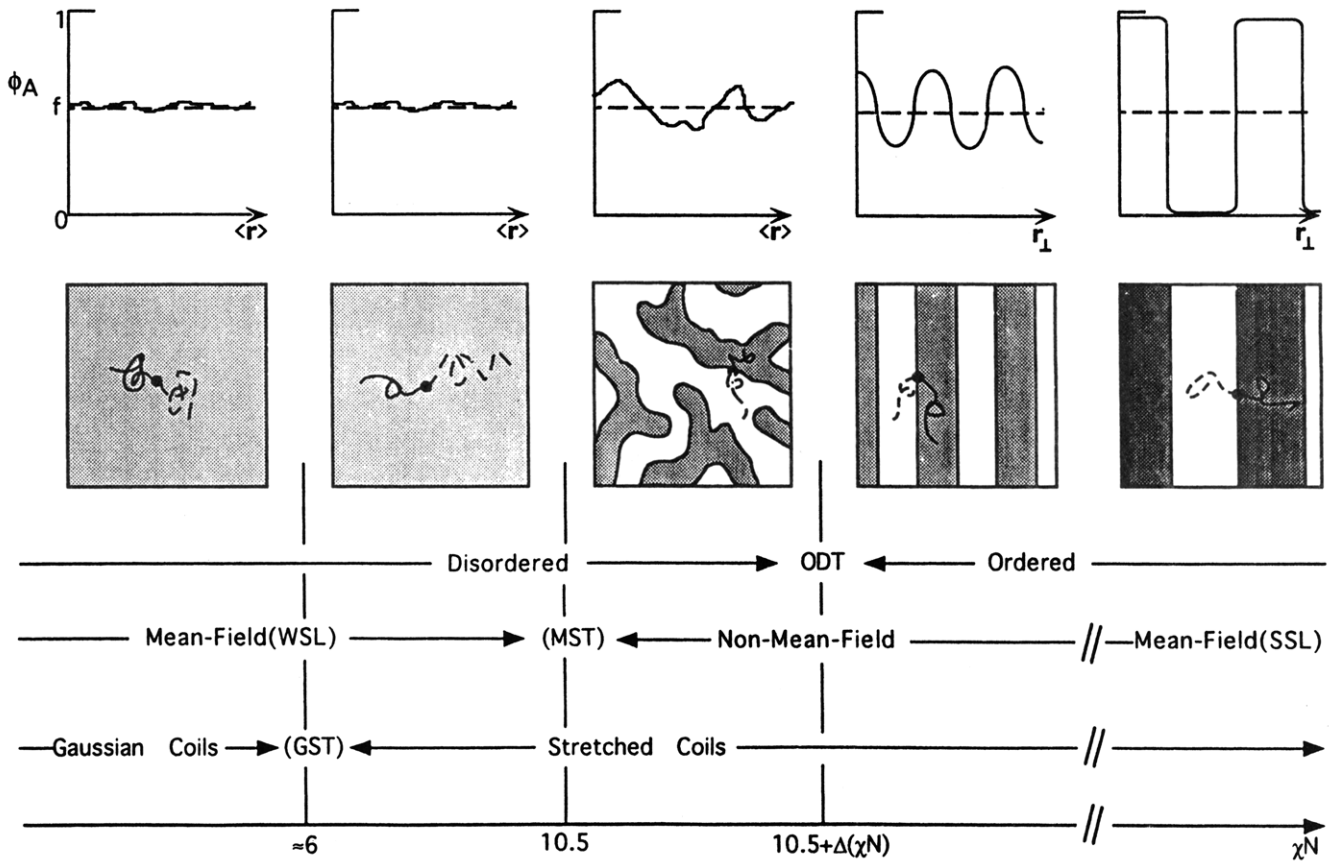

Figure 16. Illustration of the five regimes between the weak segregation (WSL) and strong segregation (SSL) limits for diblock copolymer melts. Upper sketches of ϕ_A versus r provide a qualitative sense of the variation in the amplitude of the local composition as a function of χN. Lower sketches depict the corresponding spatial patterns associated with each regime. $(\chi N)_{GST}$ was obtained from a prior publication,[43] and we assume here that $(\chi N)_x \approx (\chi N)_{MST}$ (see text).

mers were characterized by a broad crossover regime with $d \sim N^{4/5}$. The onset of this behavior occurred well into the disordered state and was denoted the Gaussian-to-stretched (coil) transition (GST). (Actually, the GST is a crossover point and not a true (thermodynamic) transition like the ODT.) Below $(\chi N)_{GST}$ we found $q^* \sim N^{-1/2}$, i.e., Gaussian coil behavior. Extrapolation of the Gaussian coil and crossover branches of the ln q^* versus ln N scaling plot leads to a crossover point at $(\chi N)_{GST} \approx 6$. This value is well below the limit $(\chi N)_x = 10.8$ reported here.

Although the present study did not extend to $\chi N = (\chi N)_{GST}$, non-Gaussian scaling between $(\chi N)_x$ and $(\chi N)_{GST}$ is consistent with the observation that $\partial \ln(q^*)/\partial T$ is larger than $-\partial \ln(R_g)/\partial T$ for the respective homopolymers in all three systems for $T > T_x$. Furthermore, based on our identification of the mean-field to non-mean-field transition, we can interpret the $T > T_x$ and $q > q^*$ SANS results for PE–PEP–6H (Figure 11) in terms of chain stretching, rather than local segregation, i.e., $\phi \cong f$ in eq 9. This indicates that at 159 °C the block copolymer molecules are stretched approximately 22% over the unperturbed Gaussian coil dimension, in good agreement with our earlier result for the PEP–PEE system.[53] A similar picture has been presented by Stühn et al.[9] based on a study of polystyrene–polyisoprene diblock copolymers.

Thus, there appear to be three well-defined regimes in the disordered state: (i) $\chi N < (\chi N)_{GST}$, mean field with Gaussian scaling; (ii) $(\chi N)_{GST} < \chi N < (\chi N)_x$, mean field with non-Gaussian (crossover) scaling; (iii) $(\chi N)_x < \chi N < (\chi N)_{ODT}$, non-mean-field with non-Gaussian (crossover) scaling. In addition, there are two ordered state regimes: (iv) $(\chi N)_{ODT} < \chi N < (\chi N)_{SSL}$, non-mean-field with crossover scaling; (v) $\chi N = (\chi N)_{SSL}$, mean field with asymptotic stretched chain scaling. These five states, from WSL to SSL are illustrated in Figure 16. Here we emphasize that the ODT is the only thermodynamic transition; the other regimes are separated by (continuous) crossover phenomena.

Simulation and theory have accounted for some of the findings presented here. Fried and Binder[11] report a Gaussian-to-non-Gaussian crossover at $\chi N \approx 4$ based on Monte Carlo simulations. Because they are able to "see" individual molecules, they can separate inter- from intrachain correlations, which is impossible in our experiments. As χN increases toward the ODT, Fried and Binder associate the initial deviation from Gaussian scaling with a reduction in translational and rotational freedom, followed by chain stretching. Within our experimental, and their computational, errors these results are rather consistent.

Barrat and Fredrickson[12] have modified the original BLFH fluctuation theory to account for the shift in the structure factor peak position near the order–disorder transition. The modified theory anticipates a significant departure from Gaussian statistics for finite molecular weights in the disordered state and that local segregation between monomers from opposing blocks should result in an overall increase in the copolymer radius-of-gyration, i.e., chain stretching. They also indicated that as χN increases in the vicinity of the ODT diblock chains assume a more "dumbbell" shape. Overall, the predictions of Barrat and Fredrickson are also supported by our work.

V. Summary and Conclusions

Several saturated hydrocarbon diblock copolymers were examined with small-angle neutron scattering (SANS) and dynamic mechanical spectroscopy (rheology) techniques near the order–disorder transition (ODT). In the ordered state, SANS experiments on both isotropic (quenched) and anisotropic (shear-oriented) specimens revealed that the compositionally symmetric ($f = 1/2$) diblocks arrange in a lamellar morphology. As the diblocks were heated toward T_{ODT} the lamellae softened, and composition fluctuations and conformational asymmetry drove the lamellae to distort. In the disordered state, SANS and rheology experiments demonstrated that composition fluctuation effects decrease with increasing chain size ($\bar{N}$). Fluctuation effects were observed in PE–PEE ($\bar{N} = 0.33 \times 10^4$) and PEP–PEE ($\bar{N} = 0.43 \times 10^4$) diblocks up to 75 °C above the order–disorder transition, while a PE–PEP diblock ($\bar{N} = 2.8 \times 10^4$) exhibited fluctuation effects only within 10 °C of the ODT. We identify the range of fluctuations with a type of Ginzburg criterion, $\Delta(\chi N) = (\chi N)_{ODT} - (\chi N)_x$. For PEP–PEE and PE–PEE $\Delta(\chi N) \cong 2.4$, while for PE–PEP $\Delta(\chi N) \cong 1.1$, and in all three systems $(\chi N)_x = 10.8 \pm 0.2$, consistent with the fluctuation theory of Fredrickson and Helfand.[3]

Complimentary to these composition fluctuation effects are conformational changes that are manifested in the magnitude and temperature dependence of the peak scattering wave vector, q^*, and $q > q^*$ scattering intensities. Three conformationally distinct disordered state regimes have been identified. For $(\chi N) < (\chi N)_{GST}$, the weak segregation limit (WSL), Gaussian coil behavior is observed, where $(\chi N)_{GST} \approx 6$. Between $(\chi N)_{GST}$ and $(\chi N)_x$ chain stretching and/or nonrandom placement leads to non-Gaussian scaling of q^* with N, and $\partial \ln q^*/\partial T > -\partial \ln R_g/\partial T$ where R_g is the unperturbed radius of gyration. This non-Gaussian behavior persists near the ODT, with $\partial \ln q^*/\partial T$ attaining the largest value when $(\chi N)_x < (\chi N) < (\chi N)_{ODT}$. There is no noticeable variation in q^* or $\partial \ln q^*/\partial T$ at the ODT. Two additional ordered state conformational regimes, near T_{ODT} and in the strong segregation limit (SSL), complete the overall picture of order and disorder in symmetric diblock copolymer melts.

Acknowledgment. This research was funded by the Air Force Office of Scientific Research (AFOSR-90-0207 and AF/F49620-93) and by the Center for Interfacial Engineering, an NSF Engineering Research Center. F.S.B. and K.A. also benefited from a NATO travel grant.

Appendix: Determining $\chi(T)$ from T_{ODT}

We previously reported[18] $\chi(T)$ for the PE–PEP, PEP–PEE, and PE–PEE diblocks by using the mean-field result $\chi_{ODT} = 10.5/N_n$ and rheologically-determined ODT temperatures together with N_n. In this paper a similar calculation is performed using the BLFH prediction,

$$(\chi N)_{ODT} = 10.5 + 41.0\bar{N}^{-1/3} \quad (f = 0.50) \qquad \text{(A-1)}$$

for the PE–PEP and PE–PEE diblocks and

$$(\chi N)_{ODT} = 10.7 + 43.16\bar{N}^{-1/3} \quad (f = 0.55) \qquad \text{(A-2)}$$

for the PEP–PEE materials, with $\bar{N} = N_n a^6 v^{-2}$ where a and v are the statistical segment length and segment volume, respectively. A common segment volume (in Å^3), based on a typical polyolefin thermal expansivity is defined as

$$v = 108 \exp[6.85 \times 10^{-4}(T - 25\ °C)]$$

On the basis of experimentally determined statistical segment lengths and thermal expansivities[32] and our definition of v, we arrive at (in Å)

$$a_{PE} = 8.8 \exp[-0.58 \times 10^{-3}(T - 25\ °C)] \qquad \text{(A-3)}$$

$$a_{PEP} = 7.2 \exp[-0.58 \times 10^{-3}(T - 25\ °C)] \qquad \text{(A-4)}$$

$$a_{PEE} = 5.0 \exp[+0.2 \times 10^{-3}(T - 25\ °C)] \qquad \text{(A-5)}$$

$\langle a \rangle$ for the diblocks was estimated using these values and the Gaussian approximation (eq 8). The T_{ODT} versus N_n data listed in Table 1 were reduced to χ_{ODT} versus T_{ODT} using the appropriate fluctuation theory expression for $(\chi N)_{ODT}$, from which $\chi(T)$ was extracted:

$$\chi_{PE-PEP} = 10.25/T - 1.86 \times 10^{-2} \qquad \text{(A-6)}$$

$$\chi_{PEP-PEE} = 4.46/T + 2.1 \times 10^{-3} \qquad \text{(A-7)}$$

$$\chi_{PE-PEE} = 15.0/T - 5.5 \times 10^{-3} \qquad \text{(A-8)}$$

In order to ensure that T_{ODT} for PE–PEP–6H, PEP–PEE–14H, and PE–PEE–8H was quantitatively matched by $\chi(T)$, the constant term in these expressions was adjusted slightly, yielding

$$\chi_{PE-PEP-6H} = 10.25/T - 1.9 \times 10^{-2} \qquad \text{(A-9)}$$

$$\chi_{PEP-PEE-14H} = 4.46/T + 1.5 \times 10^{-2} \qquad \text{(A-10)}$$

$$\chi_{PE-PEE-8H} = 15.0/T - 5.5 \times 10^{-3} \qquad \text{(A-11)}$$

These expressions were used in calculating $(\chi N)_{ODT}$ and $(\chi N)_x$ as listed in Table 2.

References and Notes

(1) Bates, F. S.; Hartney, M. A. *Macromolecules* **1985**, *18*, 2478.
(2) Leibler, L. *Macromolecules* **1980**, *13*, 1602.
(3) Fredrickson, G. H.; Helfand, E. *J. Chem. Phys.* **1987**, *87*, 697.
(4) Bates, F. S.; Rosedale, J. H.; Bair, H. E.; Russell, T. P. *Macromolecules* **1989**, *22*, 2557.
(5) Bates, F. S.; Rosedale, J. H.; Fredrickson, G. H.; Glinka, C. J. *Phys. Rev. Lett.* **1988**, *61*, 2229.
(6) Bates, F. S.; Rosedale, J. H.; Fredrickson, G. H. *J. Chem. Phys.* **1990**, *92*, 6255.
(7) Bates, F. S.; Fredrickson, G. H. *Annu. Rev. Phys. Chem.* **1990**, *41*, 525.
(8) Rosedale, J. H.; Bates, F. S. *Macromolecules* **1990**, *23*, 2329.
(9) Stühn, B.; Mutter, R.; Albrecht, T. *Europhys. Lett.* **1992**, *18*, 427.
(10) Fried, H.; Binder, K. *J. Chem. Phys.* **1991**, *94*, 8349.
(11) Fried, H.; Binder, K. *Europhys. Lett.* **1991**, *16*, 237.
(12) Minchau, B.; Dünweg, B.; Binder, K. *Polym. Commun.* **1990**, *31*, 348.
(13) Barrat, J.-L.; Fredrickson, G. H. *J. Chem. Phys.* **1991**, *95*, 1281.
(14) Mayes, A. M.; Olvera de la Cruz, M. *J. Chem. Phys.* **1991**, *95*, 4670.
(15) Melenkevitz, J.; Muthukumar, M. *Macromolecules* **1991**, *24*, 4199.
(16) Brazovskii, S. A. *Sov. Phys. JETP* **1975**, *41*, 85.
(17) Schwahn, D.; Mortensen, K.; Yee-Madeira, Y. *Phys. Rev. Lett.* **1987**, *58*, 1544.
(18) Bates, F. S.; Schulz, M. F.; Rosedale, J. H.; Almdal, K. *Macromolecules* **1992**, *25*, 5547.
(19) Bates, F. S.; Fredrickson, G. H. *Macromolecules*, in press.

(20) Vavasour, J. D.; Whitmore, M. D. *Macromolecules* **1993**, *26*, 7070.
(21) Rosedale, J. H.; Bates, F. S. *J. Am. Chem. Soc.* **1988**, *110*, 3542.
(22) Nicholson, J. C.; Crist, B. *Macromolecules* **1989**, *22*, 1704.
(23) We are grateful to G. Krausch and E. Kramer for conducting this measurement.
(24) Almdal, K.; Bates, F. S.; Mortensen, K. *J. Chem. Phys.* **1992**, *96*, 9122.
(25) Almdal, K.; Koppi, K. A.; Bates, F. S.; Mortensen, K. *Macromolecules* **1992**, *25*, 1743.
(26) Amundson, K.; Helfand, E.; Patel, S. S.; Quan, X.; Smith, S. D. *Macromolecules* **1992**, *25*, 1935.
(27) Koppi, K. A.; Tirrell, M.; Bates, F. S.; Almdal, K.; Colby, R. H. *J. Phys. II Fr.* **1992**, *2*, 1941.
(28) Wignall, G. D.; Bates, F. S. *J. Appl. Crystallogr.* **1987**, *20*, 28.
(29) Pedersen, J. S.; Posselt, D.; Mortensen, J. *J. Appl. Crystallogr.* **1990**, *23*, 321.
(30) Benoit, H.; Hadziioannou, G. *Macromolecules* **1988**, *21*, 1449.
(31) Tang, H.; Freed, K. F. *Macromolecules* **1991**, *24*, 958.
(32) Fetters, L. J.; Lohse, D. J.; Richter, D.; Witten, T. A.; Zirkel, A. *Macromolecules*, in press.
(33) Amundson, K.; Helfand, E. *Macromolecules* **1993**, *26*, 1324.
(34) Fredrickson, G. H.; Binder, K. *J. Chem. Phys.* **1989**, *91*, 7265.
(35) de Gennes, P.-G. *The Physics of Liquid Crystals*; Clarendon Press: Oxford, U.K., 1974.
(36) Foster, M. D.; Sikka, M.; Singh, N.; Bates, F. S.; Satija, S. K.; Majkrzak, C. F. *J. Chem. Phys.* **1992**, *96*, 8605.
(37) Olvera de la Cruz, M. *Phys. Rev. Lett.* **1991**, *67*, 85.
(38) Hamley, I. W.; Koppi, K. A.; Rosedale, J. H.; Bates, F. S.; Almdal, K.; Mortensen, K. *Macromolecules* **1993**, *26*, 5959.
(39) Han, C. D.; Baek, D. M.; Kim, J. K. *Macromolecules* **1990**, *23*, 561.
(40) Winey, K. I.; Gobran, D. A.; Xu, Z.; Fetters, L. J.; Thomas, E. L. *Macromolecules* **1994**, *27*, 2392.
(41) Owens, J. N.; Gancarz, I. S.; Koberstein, J. T.; Russell, T. P. *Macromolecules* **1989**, *22*, 3380.
(42) Hashimoto, T.; Ijichi, Y.; Fetters, L. J. *J. Chem. Phys.* **1988**, *89*, 2463.
(43) Ehlich, D.; Takenaka, M.; Hashimoto, T. *Macromolecules* **1993**, *26*, 492.
(44) Bates, F. S.; Fetters, L. J.; Wignall, G. D. *Macromolecules* **1988**, *21*, 1086.
(45) Gehlsen, M. D.; Rosedale, J. H.; Bates, F. S.; Wignall, G. D.; Hansen, L.; Almdal, K. *Phys. Rev. Lett.* **1992**, *68*, 2452.
(46) Koppi, K.; Tirrell, M.; Bates, F. S. *Phys. Rev. Lett.* **1993**, *70*, 1449.
(47) The authors are grateful to Glenn Fredrickson for providing this derivation of the composition fluctuation amplitude associated with the theory described in ref 3.
(48) Binder, K. *Phys. Rev. A* **1984**, *29*, 341.
(49) Cates, M. E.; Milner, S. T. *Phys. Rev. Lett.* **1989**, *62*, 1856.
(50) Marques, C. M.; Cates, M. E. *J. Phys. (Fr.)* **1990**, *51*, 1733.
(51) Semenov, A. N. *Sov. Phys. JETP* **1985**, *61*, 733.
(52) Helfand, E.; Wasserman, Z. R. In *Developments in Block Copolymers—1*; Goodman, I., Ed.; Applied Science: New York, 1982.
(53) Almdal, K.; Rosedale, J. H.; Bates, F. S.; Wignall, G. D.; Fredrickson, G. H. *Phys. Rev. Lett.* **1990**, *65*, 1112.

MA945062M